Characterizing the Parameter Space of an Oxygen Gradient between Hypoxic and Normoxic Gas Networks

By
Esther Jeeyoung Shin
B.S., Georgia Institute of Technology, Atlanta, GA, 2014

THESIS

Submitted as partial fulfillment of the requirements
for the degree of Master of Science in Bioengineering
in the Graduate College of the
University of Illinois at Chicago, 2016.
Chicago, Illinois

Thesis Committee:

David Eddington, Chair and Advisor
Salman Khetani
Richard Magin

This thesis is dedicated to my parents and sister who have endured through making me who I am today, through all the struggles and uncertainties.

This is also dedicated to the friends and church family that have stood by me and checked in on me when I went off-the-grid or when I wasn't the easiest person to stand by.

Lastly, this thesis is a true testament to the grace and ability given to me by the one and only God. Nothing would have been possible if He hadn't enabled it to be so.

ACKNOWLEDGMENTS

I would like to thank the following individuals for helping me with my research:

Dr. David Eddington - my research and thesis advisor.

Dr. Salman Khetani - part of my thesis committee.

Dr. Richard Magin - part of my thesis committee.

My laboratory colleagues for their help and support.

TABLE OF CONTENTS

LIST OF TABLES

LIST OF FIGURES

LIST OF ABBREVIATIONS

atm	Atmosphere (of pressure)
cm	Centimeter
CDA	Clean dry air
^{o}C	Degrees Celsius
DI	Deionized water
T_g	Glass transition temperature
HIF	Hypoxia inducible factor
Q	Volumetric flow rate
I	Fluorescence intensity (in presence of oxygen)
I_0	Fluorescence intensity (without oxygen)
ID	Inner diameter
IPA	Isopropanol
kPa	Kilopascal
L	Length
MPa	Megapascal
m	Meter
MEMS	Microelectromechanical systems
μm	Micrometer
mg	Milligram
mJ	Millijoule

mL	Milliliter
mm	Millimeter
mW	Milliwatt
min	Minute
OD	Outer diameter
O_2	Oxygen
PtOEPK	Platinum(II) octaethylporphyrin ketone
PDMS	Polydimethylsiloxane
PEB	Post-exposure bake
ΔP	Change in pressure
K_q	Quenching constant
r	Radius
RPM	Revolutions per minute
s	Second
G	Shear modulus
Silane	Tridecafluoro-1, 1,2,2-TetraHydro Octyl-1-Tricholosilane
UV	Ultraviolet
μ	Viscosity
W	Watts

SUMMARY

Microfluidics has been growing in popularity for lab-on-a-chip applications and is a versatile platform for biologic studies. However, there is still much research to be done in understanding and achieving precise manipulation of these devices. A prominent example of this is in using microfluidics to study gas control in hypoxic and normoxic dual condition environments. The hypothesis is that by manipulating different parameters in the device design, the oxygen gradient profile generated in the dual condition devices can be precisely manipulated because of the difference in the resistance values. These series of experiments show that there does not seem to be a way to change these gradient profiles by using different device designs to create different resistances in the channel environments. Regardless of the change in the design of the device, the same oxygen profile is observed, indicating that the geometry of the device design does not play a major role in the generation of the oxygen gradient. Extensive experiments were performed to show the generation of identical oxygen profile landscapes, even in a very low-resistance environment. This knowledge, which was found contrary to theoretical hypotheses, can aide researchers studying oxygen control and give further insight into the effect and manipulation of microfluidic device design.

CHAPTER I: INTRODUCTION AND BACKGROUND

1.1 - Microfluidics

1.1.1 - History and origin of microfluidics

Microfluidics is defined as "the science and engineering of systems in which fluid behavior differs from conventional flow theory primarily due to the small length scale of the system." Although technology has become increasingly miniaturized, the widespread use of nonelectronic microfluidics was not seen until the late 1980s with the development of micropumps, microflow sensors, and microvalves. The term "microfluidics," and terms such as microelectromechanical systems (MEMS), "MEMS-fluidics" and "Bio-MEMS," were coined to specifically describe the research discipline of microscopic transport phenomena and fluid-based devices. The discipline of microfluidics refers not to the overall device size, but to the length scale that determines the behavior of the flow in the device(1). One of the major advantages of using microfluidics is that it exhibits mainly laminar flow in the channels, contrary to macro-flow theory which is characterized mainly as turbulent flow. The presence of laminar flow indicates that any mixing in the channels is a result of diffusion across the membrane or molecules(2), and not as a result of mixing from turbulent flow. The discipline has been growing in popularity because of its ability to manipulate flow configurations on the scale of microns, the search for cheap and simple analytical devices, and the potential of microscale devices in physical, chemical, and biological processes(3). Although microfluidics is widely used for liquid flow applications, it is also used to manipulate gas flow in the channels to create physiologically accurate environments for cellular studies. This study utilizes the properties of microfluidics and explores the extent to

which oxygen control can be performed, ultimately to generate more physiologically accurate environments for scientific study.

1.1.2 Polydimethylsiloxane (PDMS)

One of the most common materials used for fabrication of microfluidic devices is polydimethylsiloxane (PDMS). One of the main advantages to the usage of PDMS is its ability to be manipulated and molded rapidly on the micro-scale(4). The mechanical properties that contribute to the usage of PDMS are its optical clarity which contributes to imaging applications, high gas permeability of around 5200$\frac{cm^3 \cdot mm}{m^2 \cdot day \cdot atm}$ (5) allowing for gas flow experiments (6, 7) and the ability to absorb water and hydrophic soluble factors(8-11). In addition, PDMS has a low glass transition temperature with $T_g \approx$ -125^{o}C (12), a shear modulus G between 100kPa and 3MPa indicating a special range of flexibility (12), small temperature variations of the physical constants (13), high dielectric strength of about 14$\frac{V}{\mu m}$ (13), high compressibility (7), usability over a wide temperature range of about -100^{o}C to 100^{o}C (14), and a non-toxic nature(7).

PDMS designs are typically used with soft-lithography molds for rapid prototyping(15). However, this method of fabrication causes the device to have high hydrophobicity which could cause problems in biological processes and studies(16). Although there are chemicals and other applications that can be used to counteract the hydrophobicity of the constructed device, this is still considered to be a major limitation of using PDMS for microfluidic devices. Despite this, PDMS is used for many different purposes because it provides a versatile platform for research studies.

1.2 - Dual condition systems

1.2.1 - Hypoxia

Hypoxia is defined as "a reduction in the normal level of tissue oxygen tension" and is prevalent in conditions such as vascular disease, pulmonary disease, and cancer(17). Hypoxic conditions are important because of its role in the differentiation of stem and precursor cells(18). Other research has also shown that a reduction in oxygen tension causes changes to gene expression by affecting different cellular pathways, notably angiogenesis, metabolism, migration, proliferation, differentiation, and apoptosis(19). Hypoxic conditions are almost always a result of the transcriptional activity of hypoxia inducible factors (HIF)(20). HIF-1α, a subunit of the HIF "family" has been well characterized and found to be upregulated in hypoxic environments. Research indicates that the HIF-1α subunit plays a major role in oxygen homeostasis and disease pathophysiology(21). To examine and further research on the HIF genes, a stable platform such as microfluidics that can be used to mimic physiological system environments must also be further developed, which this study looks to contribute to.

1.2.2 - Oxygen gradients

Oxygen control is an important component in numerous biologic applications such as stem cell differentiation(22), angiogenesis(23), embryonic development(22), and cellular growth(24). The human body is composed of a relatively large range of oxygen concentrations(25). Although the environmental air is composed of 21% oxygen, the normal level of oxygen (normoxia) found in the organs and tissues is much lower, measuring between 2-9%(18). Though this range would be characterized as hypoxic by the given definition, this is the normal physiological oxygen concentrations found in body systems (and thus is not referred to as hypoxic). This is but a

singular example of the more complicated characterization of the body's gas composition. Although these individual conditions of hypoxia and normoxia are important, the importance of oxygen gradients in the body have been growing in prevalence. Oxygen gradients are considered to play a significant role in maintaining homeostasis and inducing acute cellular responses in body systems(26). It is difficult to create accurate and stable oxygen gradients in a system for study. Current solutions rely on specially mixed gas concentration oxygen tanks (though the cost of these can become relatively high), special incubators, or different platforms for mixing. There is a need for an inexpensive method to create physiologically accurate oxygen gradient environments for cellular study. This study seeks to provide insight into the incidence and precise manipulation of oxygen gradients through relatively cheap means of design modifications.

1.3 - Current uses and applications

1.3.1 - Microfluidics

Microfluidics has its most frequent usage in laboratory and research settings. Research has shown that these devices are useful in studying and mimicking biophysical and biochemical microenvironments for the study of cells *in vitro*(27-31). Microfluidic devices have also started to emerge as flow control systems, microseparators (1), hypoxic activation chambers (32), cell culture and chemical analysis (33), and many others. There is an increasing number of laboratory and research applications emerging as more is understood about the nature of microfluidics. Although most commonly used in research settings, its application has also started to emerge in point-of-care diagnostic devices (immunoanalysis, cell analysis, etc.) because of its rapid and relatively cheap cost of fabrication(34).

1.3.2 - Oxygen gradients

Microfluidics can be used to generate oxygen gradients to provide a close representation of physiological system environments that cannot typically be done with existing methods used to generate hypoxic environments(19). Although there are currently various devices and set-ups to create gas variable environments to study cellular behavior in different conditions, there are many shortcomings to existing methods such as high cost for specialized equipment, limitations to the length of time for the study, and many others. Conventional incubators generate different gas mixtures of oxygen, nitrogen, and carbon dioxide mix the gases in a predefined ratio to get the desired oxygen percentage. This method is limited in its longevity to maintain these systems that do not generate oxygen gradients that are of interest for physiological studies(35). Hypoxia work stations and hypoxia chambers are among the most common methods used to study cellular environments under low oxygen concentrations. However, similar to conventional incubators, oxygen gradients cannot be generated using hypoxic workstations or chambers. Hypoxic work stations and chambers also require bulky and specialized equipment that can get costly. Microfluidics provides a platform that can be used over extended periods of time to generate and study hypoxic environments by providing an environment for tight oxygen control(19). Different labs have been exploring different procedures to create and manipulate oxygen environments. Although the following examples generate oxygen gradients in distinctly different methods, all these studies seem to agree that microfluidics is ideal for generating these oxygen gradients of interest. A study conducted by Mehta et al generated an elastomer bioreactor to generate axial oxygen gradients caused by the uptake of oxygen by the cells(36). Adler et al generated different oxygen gradients using a system of "arbitrary shapes(37)." Still others such as Chen et al utilized spatially confined chemical reactions to generate oxygen gradients in the cell

culture(38). The multitude of different approaches shows the still unmet need for a universal platform and method to create oxygen gradient environments for scientific research and cellular study.

1.4 - Research purpose

Although a vast amount of research has been done in the field of microfluidics and the generation of oxygen gradients in the devices, there are still many basics that are not fully understood. In light of the growing applications and need for devices that precisely manipulate gas control to generate a realistic physiological environment, the understanding of device design manipulation and its effect on the gas flow in the system is still under-developed. Oxygen conditions are extremely important for the study of cellular processes. This study and series of experiments seek to elucidate the effect of different resistance values caused by different device designs on the oxygen gradient profile. A dual condition device is studied to provide both environments of hypoxia and normoxia and examine the effects of the different designs on the oxygen gradient profile observed in the space between the two chambers. This gradient is important in providing an environment that can be potentially used for cellular studies. PDMS has been proven to be a reliable platform for oxygen studies because of its high gas permeability as well as its other physical properties. As such, PDMS is one of the most common materials used for microfluidic device construction and is the material used in these experiments. By gaining this understanding of the effect of device design on the oxygen gradient, it will help to provide insight into device manipulation to ultimately save resources (time and money) when working on projects that require gas flow manipulation and the generation of oxygen gradients on the micro-scale.

CHAPTER II: MATERIALS AND METHODS

2.1 - Device fabrication

Two different device designs were explored to characterize the effect of resistance and different parameters on the oxygen profile of a dual-condition device. The dual-condition device is defined by two different oxygen concentrations run through each section of the device. The first iteration of designs was a serpentine channel design with differing parameters and is shown with the parameters defined in Figure 2.1. The inlet and outlet sides are also labeled, with the inlet side always leading directly to the gap between the dual condition channels.

An expanded schematic of the serpentine channel designs are shown in Figures 2.2, 2.3, and 2.4, broken down into the different parameters examined and described in detail below**.** The second design was an open-well channel with supporting posts that had different spacing between the dual condition sections as shown in Figure 2.5, described in more detail below. These designs were expected to have substantially lower resistances in the device channels, which was important since resistance was considered to be the possible manipulative factor for oxygen gradient profiling.

A)

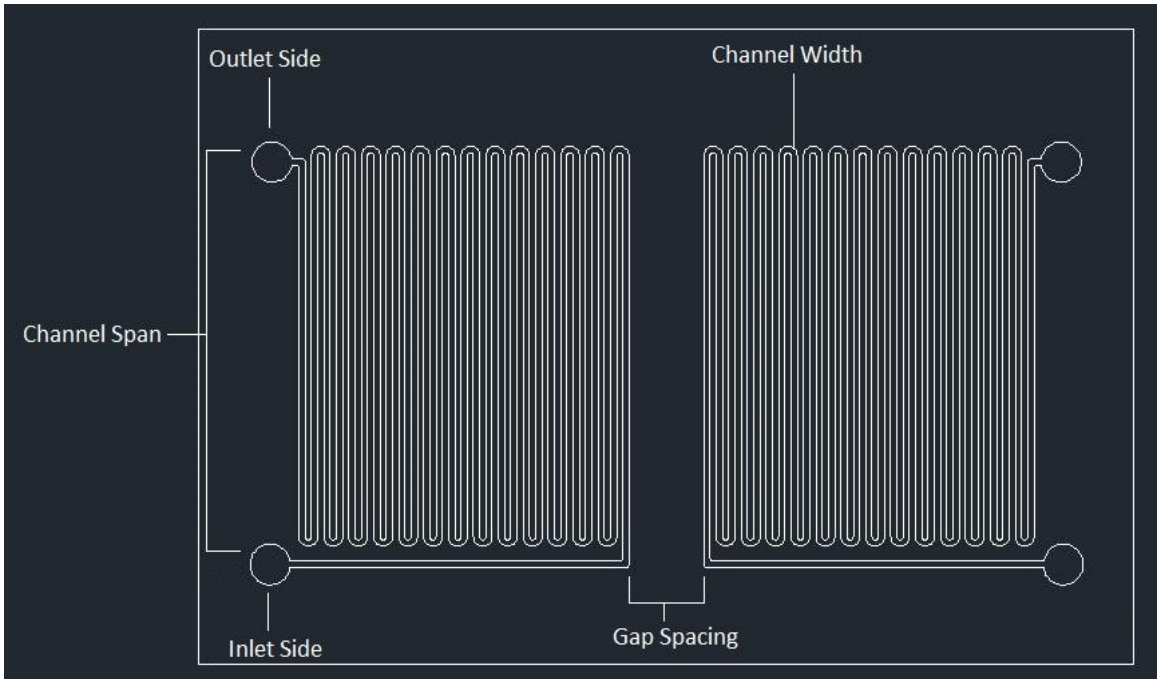

B)

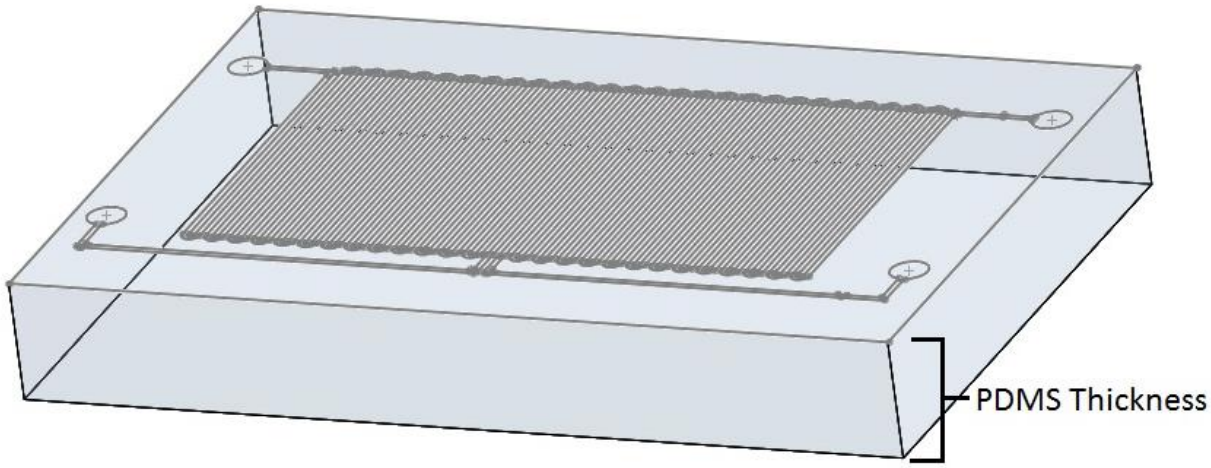

Figure 2.1. Serpentine channel device schematic defining the parameters of interest explored in the experiment. A) Schematic for the definitions of spacing, span, and width.
B) Schematic for the definition of thickness.

2.1.1 - Serpentine channel device

The serpentine device design was constructed to house a dual condition binary landscape, previously described in Rexius et al, where different oxygen landscapes were generated using different device designs. Based on this paper, the 30mm span serpentine channel design was considered to be the standard design utilized, unless otherwise stated(32). The designs were altered to examine the effect of the change in a singular physical factor on the slope of the observed gradient when run under dual conditions. Based on the Hagen-Poiseuille equation for resistance shown below in Equation 2.1 and the assumption that the resistance was a driving factor in generating the oxygen gradient, the different parameters were determined to produce different resistance values in the channels.

$$\Delta P = \frac{8\mu LQ}{\pi r^4} \tag{2.1}$$

where ΔP is the change in pressure , μ is the viscosity, L is the length, Q is the flow rate, and r is the radius. Although the assumptions that follow the Hagen-Poiseuille equation are not necessarily met in microfluidics, the different designs focused on changing one of the variables in the equation to examine a resistance change and a differing oxygen gradient profile. Some of the parameters that were looked at were the span of the device, the thickness of the device material, the spacing between the two channel conditions, and the width of the channels, as defined in Figure 2.1. The channel span referred to the length of the loop of a serpentine channel and spanned over 10mm, 20mm, 30mm, and 40mm with differing channel depths of 140μm and 265μm, as shown in Figure 2.2. The device thickness referred to the amount of polydimethylsiloxane (PDMS) poured onto the 30mm span, 140μm deep fabricated masters. The

thicknesses examined were 1mm, 2mm, and 4mm heights. The spacing of the channels was the distance between the dual-condition chambers, made up of a hypoxic and a normoxic region. The spacing distances observed were 0.250mm, 1mm, and 2mm as shown in Figure 2.3. Lastly, the channel widths referred to the width of the fabricated channels. The observed channel widths were 0.075mm, 0.250mm, and 0.750mm as shown in Figure 2.4.

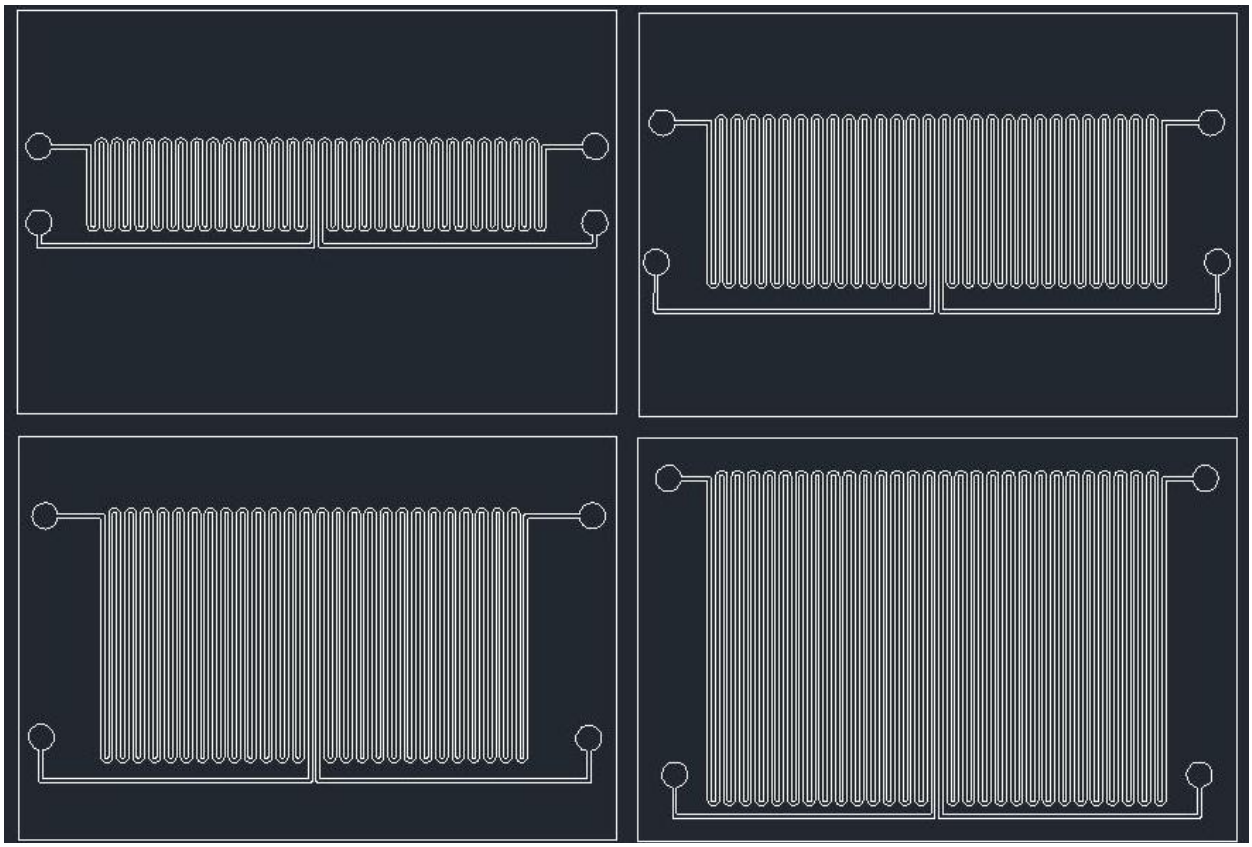

Figure 2.2. Serpentine channel span designs. The spans observed ranged from 10mm (upper left), 20mm (upper right), 30mm (considered to be the "standard" and shown in the bottom left), and 40mm (bottom right). Two different channel depths of 140μm and 265μm were examined for a different profile.

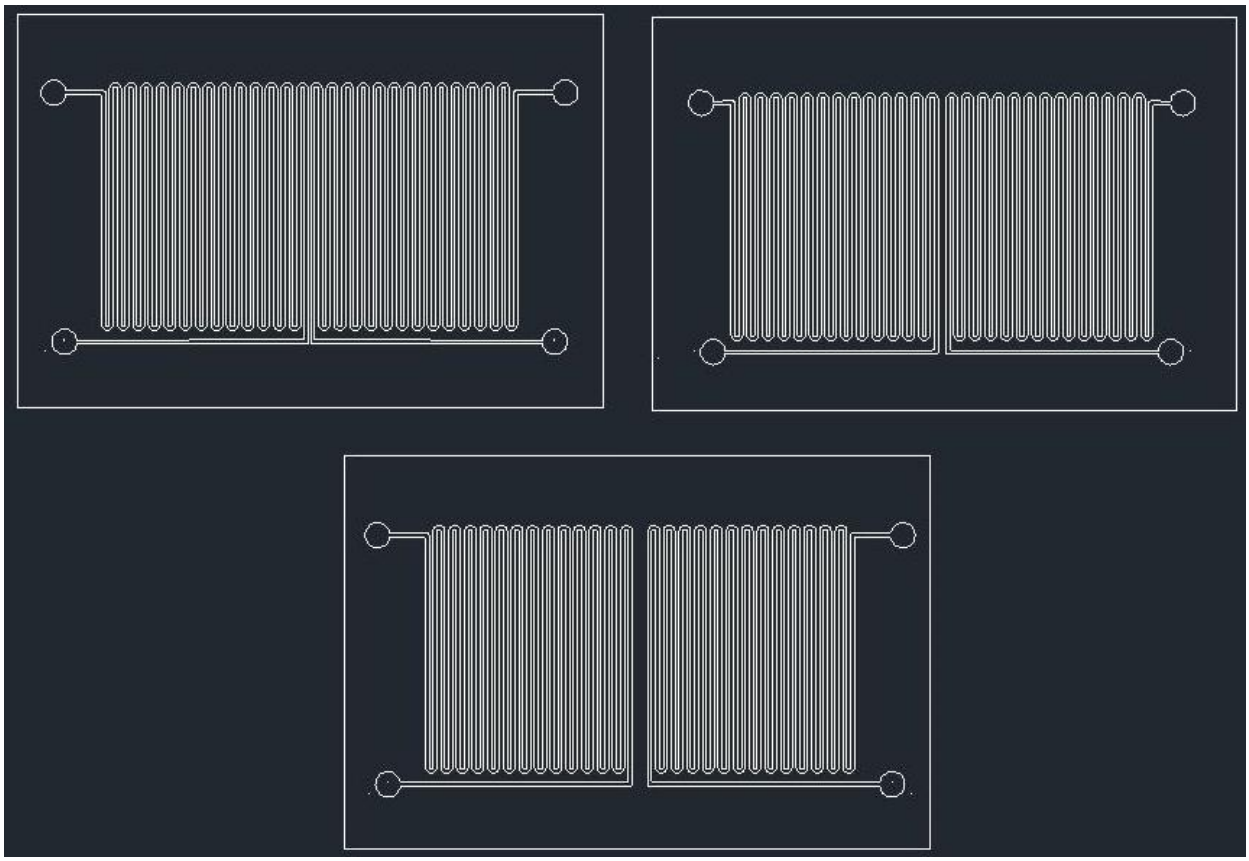

Figure 2.3. Serpentine gap spacing designs. The gap spacing referred to the distance between the hypoxic condition (left chamber) and the normoxic condition (right chamber). The observed distances were 0.250mm (upper left), 1mm (upper right), and 2mm (bottom).

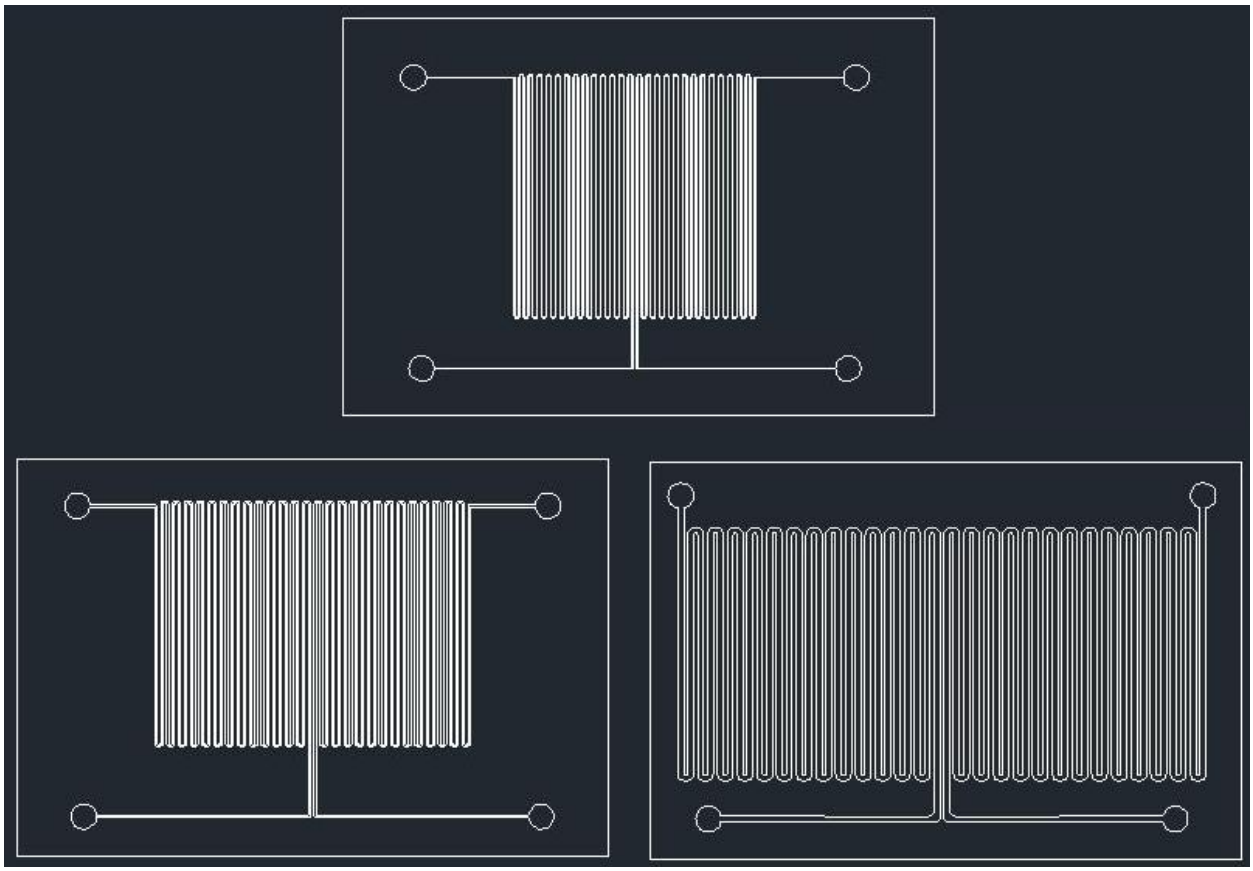

Figure 2.4. Serpentine channel width designs. The width of the channels observed were 0.075mm (above), 0.250mm (lower left), and 0.750mm (lower right).

2.1.2 - Open-well channel device

The open-well channel device design was constructed to examine a condition with reduced resistance in the channels. The dimensions of the open well designs were kept consistent with the previously mentioned serpentine channel devices. Since the design consisted of a large single channel, supporting posts were added to prevent channel collapse. The supporting posts were 500µm in diameter and were spaced 350µm apart, end to end. These posts were constructed to support the membrane layer and keep the diffusion layer from collapsing onto the channel layer system. The variable parameter of interest was the spacing between the two gas chambers. The spacing between the two chambers examined were 0.250mm and 2mm as shown in Figure 2.5.

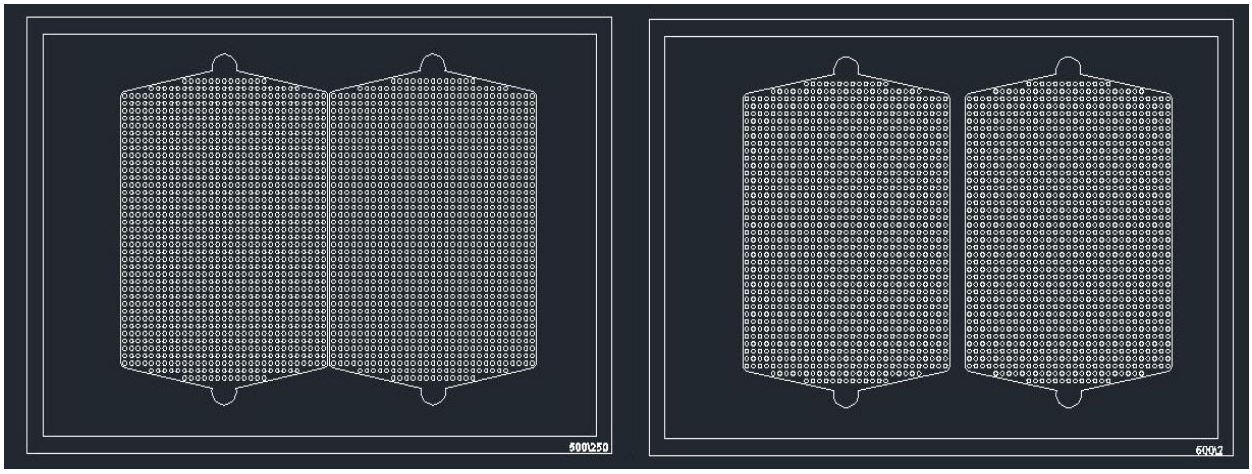

Figure 2.5. AutoCAD designs of open-well channel devices. Designs had 500µm diameter posts 350µm apart and varied gap spacing between the hypoxic and normoxic region across the devices. Spacing distances were 0.250mm (left) and 2mm (right) observed in the serpentine channel devices.

It is important to note that the dimensions of the device schematics were kept as constant as possible. In this manner, if a difference was seen in the oxygen profile, it could be attributed to a singular factor. The factors held more or less constant (unless otherwise stated in the device design descriptions above) are shown in Table 1 below:

TABLE I

DEVICE DIMENSIONS

Component	**Dimension**
Glass Slide	75mm x 50mm
Channel/Chamber Width	26.5mm
Channel/Chamber Length	31.5mm
Open-well Supporting Posts	500μm (diameter), 350μm apart
Inlet/Outlet Ports	1.6mm (radius)
Tubing	0.0625" ID, 0.125" OD
SU-8 Depth	140μm
PDMS Diffusion Layer	100μm
PDMS Spacer Layer	~2mm
Gas Flow Rate	30mL/min
Microscope Magnification	4X

2.1.3 - Platinum(II) octaethylporphyrin ketone (PtOEPK)

To make the platinum(II) octaethylporphyrin ketone (PtOEPK) oxygen fluorescence sensor, the procedure outlined in Sinkala et al was followed(39). First, 35% w/w of polystyrene/toluene was taken and mixed in a glass jar. The glass jar was then covered and placed on a shaker for 24 hours. The jar was uncovered and 1mg/mL of PtOEPK powder was added. The jar was re-covered and then placed on the shaker for another 24 hours. A 100µm thick PDMS layer was fabricated on a wafer using the spin coater set at 500RPM for 10 seconds and 800RPM for 30 seconds and then cured for 30 minutes on a 85^{o}C hot plate. Toluene was added to the wafer as well as the solution placed in the jar described above. The solution was spun in the spinner at the same RPM and the wafer was covered and cured on a 85^{o}C hot plate for 30 minutes. The constructed wafer of PtOEPK was placed in a covered petri dish, taking care to minimize its light exposure when not in use. When the PtOEPK sensor is exposed to oxygen, the sensor fluorescence is relatively low. Conversely, when the sensor is exposed to a lower oxygen concentration, the fluorescence intensity has relatively high values. An example of the layout of the sensor and the raw images that are obtained from MetaMorph® are shown in Figure 2.6.

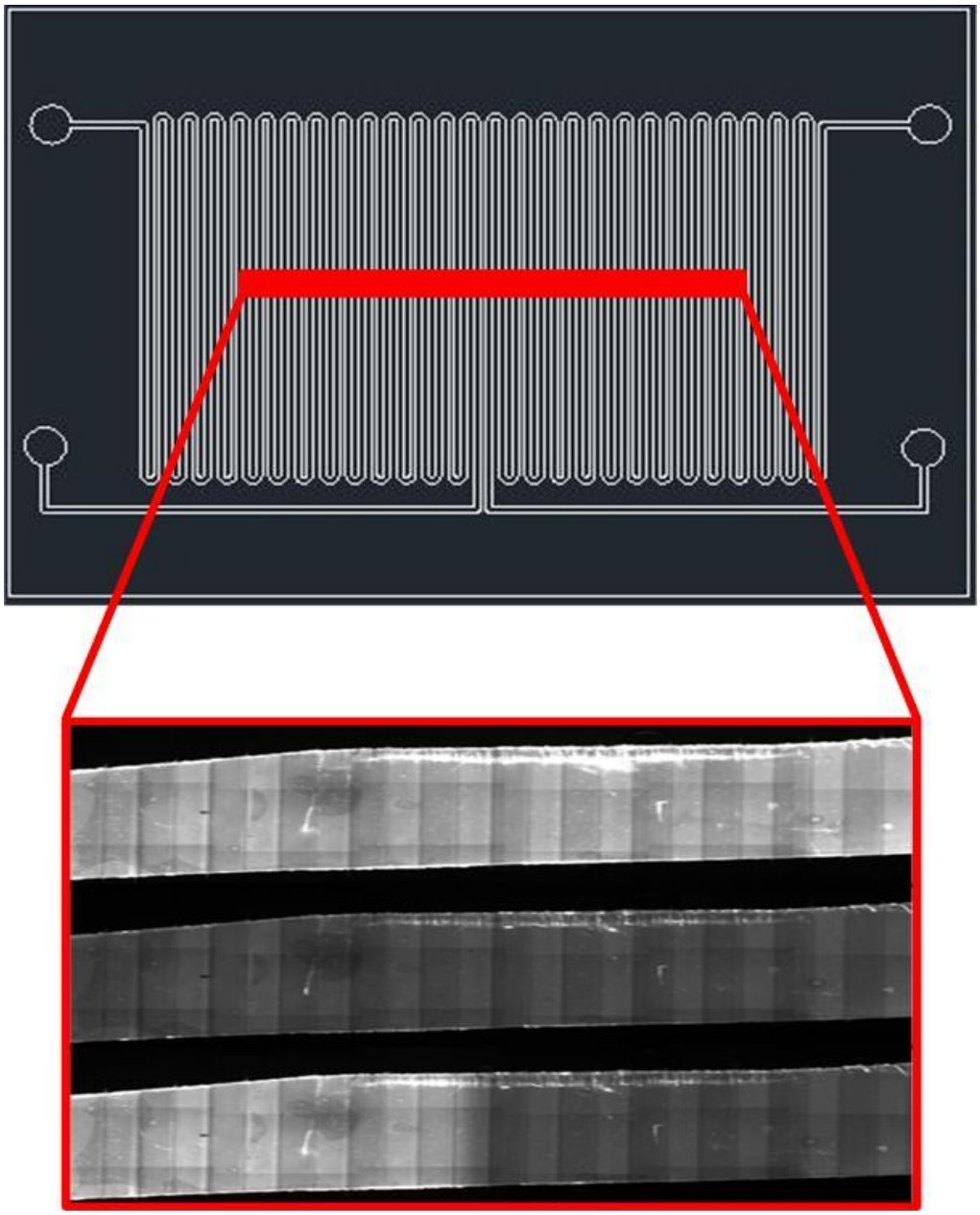

Figure 2.6. A PtOEPK sensor was used to measure oxygen fluorescence in the microfluidic channels. A sample region as shown above was taken to generate three different scans. The brightest scan on the top is for 0% oxygen condition, the second dark scan shows 21% oxygen, and the last scan shows the dual condition.

2.1.4 - Multilayer device fabrication

The microfluidic devices were fabricated using PDMS in a multilayer system. Once the photomasks were designed using AUTOCAD, the masters were constructed through standard SU-8 photolithography techniques as diagrammed in Figure 2.7 and elaborated on below.

For consistency, SU-8 2100 photoresist was used for each of the masters constructed. A 100mm diameter silicon wafer was cleaned under the hood and placed in the spinner using an aligner. The spinner was set to 500 rpm with an acceleration of 500 for 10 seconds for step 1 and 2000 rpm with an acceleration of 1500 for 30 seconds for step 2 to achieve a thickness of 140μm. A small amount of the SU-8 2100 photoresist was poured onto the center of the wafer in the spinner. The clean dry air (CDA) gas and the vacuum were turned on and the spinner was closed. After the SU-8 photoresist was spun onto the master, the wafer was carefully taken off the spinner and placed onto a hot plate set at 65^{o}C for 5 minutes as a pre-bake. It was then placed onto a 95^{o}C hot plate to softbake for 30 minutes. The wafer was covered with the top of a petri dish covered in foil during the softbake process to ensure that the photoresist film on the wafer was not exposed to any light. After the softbake, the wafer was placed on a flat surface and covered to cool.

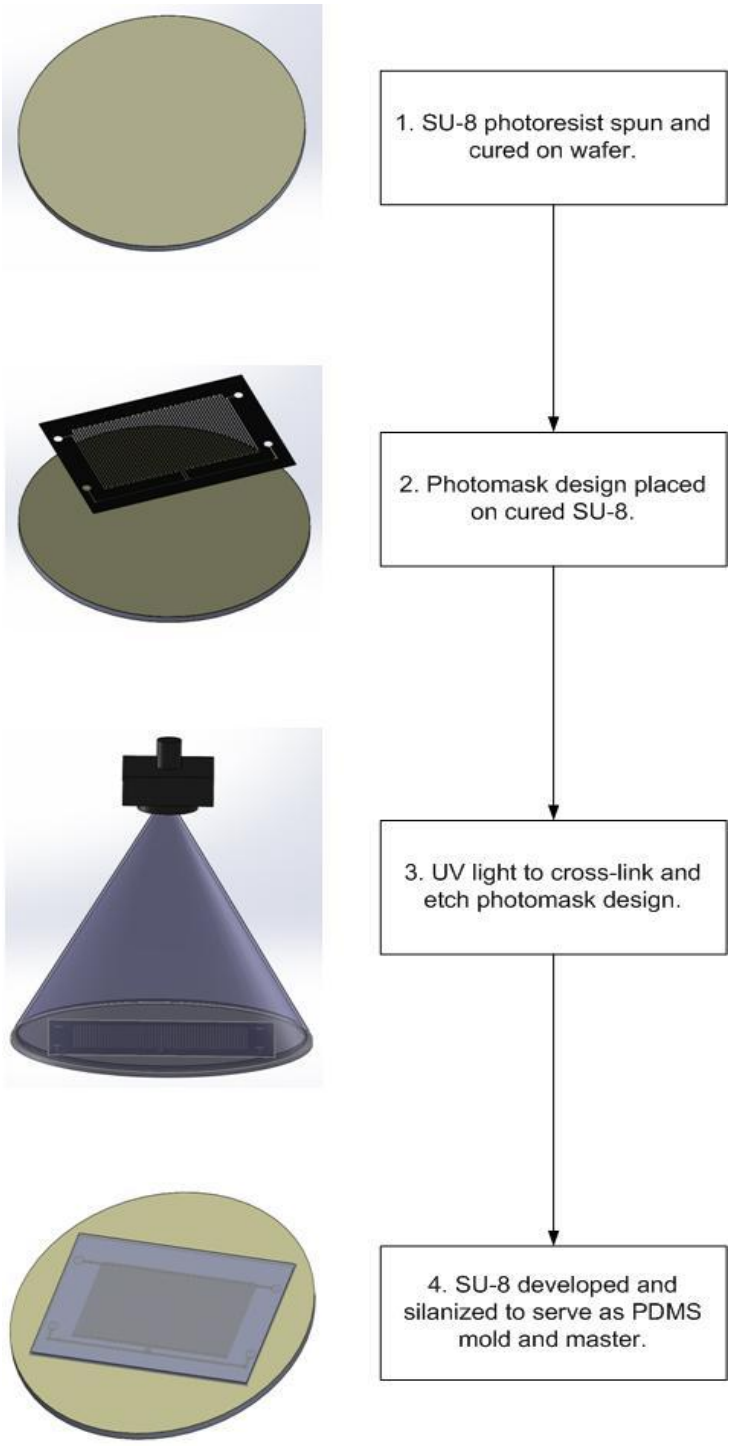

Figure 2.7. Standard SU-8 protocol was used to construct masters from mask designs. SU-8 2100 was poured onto a 100mm wafer, spin coated, and cured on hot plates. The photomask was then placed onto the cured SU-8 and exposed to UV light to selectively polymerize and form cross-links to etch the photomask design onto the SU-8 photoresist. After more baking and shaking in developer solution, the SU-8 was silanized to use as the PDMS master mold.

While the wafer was cooling, the ultraviolet (UV) exposure machine was turned on and a radiometer was used to verify the light intensity before each exposure. Glasses are worn to prevent retinal damage from UV exposure while operating this device in accordance with safety protocols. The light was aligned to the size of the 100mm wafer and the exposure time was calculated using the measured UV light intensity as shown below in Equation 2.2:

$$Exposure\ Duration = \frac{Energy\ Density}{(\frac{Lamp\ Output}{Surface\ Area})} \tag{2.2}$$

where the energy density was obtained from the SU-8 manufacturer (mJ/cm^2), the surface area represents the surface area of the wafer (78.5398 cm^2), and the lamp output was converted from mW given by the radiometer to mJ/s. The calculated exposure duration was doubled to give the correct exposure time to correctly polymerize the wafer. The cooled wafer was placed in alignment with the UV light with the photomask placed in the center of the wafer. A quartz glass disc the same size as the wafer was placed on top of the entire device. The device was selectively polymerized by the UV light according to the photomask design. Following exposure, the device was again placed on a 65^{o}C hot plate for 5 minutes and then transferred to a 95^{o}C hot plate for 12 minutes for the post-exposure bake (PEB). Following the PEB, the wafer was allowed to cool again to room temperature. In order to remove any uncross-linked polymers on the wafer, the wafer was placed in once-used SU-8 developer solution and shaken for 15 minutes. The wafer was then washed with isopropanol (IPA) and dried under nitrogen gas before being placed in new SU-8 developer solution to clean the photoresist on the wafer. This second developer was shaken for approximately 5 minutes before it was rinsed again and dried. The masters were silanized overnight in a vacuum chamber. In this silanization process, 30µL of Tridecafluoro-1,

1,2,2-TetraHydro Octyl-1-Tricholosilane (silane) solution was deposited on a glass slide in the same vacuum chamber as the developed master. This silanization process allowed for a thin layer of silane to be deposited, allowing for other chemicals to stick less effectively and not ruin the SU-8 mold design. The wafer was used as the mold for the PDMS channel layer, with the silanization allowing for the PDMS to be peeled off easily after curing. (40)

The PDMS was poured at a ratio of 10:1 of base to curing agent and spun to mix together. It was then placed for approximately 30-45 minutes in a vacuum dessicator to de-gas and remove any bubbles that formed when the mixture was poured onto the device. Once removed from the vacuum, it was placed on a hot plate at 85^{o}C to cure for about an hour and a half. The device was then carefully cut from the mold and bonded to a 100μm thick PDMS membrane. This membrane is made by placing PDMS on a wafer in a spin coater (500 RPM for 10 seconds and then 800 RPM for 30 seconds) and cured for 30 minutes at 85^{o}C. The PDMS device with the channels was plasma-bonded with the thin PDMS membrane using a handheld corona discharge device at its maximum output power of 30 Watts (W) by treating the surfaces for approximately 3 minutes. The bonded device is placed on a hot plate to cure for 30 minutes at 85^{o} C. The same process was repeated to bond the bottom of the device to a 75mm x 50mm glass slide and the top to an open-well spacer layer. The open-well spacer layer was cut to the dimensions of the 75 mm x 50 mm glass slide, with an inner rectangle approximately 10μm from each edge removed to create walls for the open-well. Inlet and outlet holes are bored through the entirety of the device with a radius of 1.6mm. Lastly, the PtOPEK sensor is placed in contact with the diffusion layer for the oxygen fluorescence imaging described below. The completed device is represented in the schematic as shown in Figure 2.8.

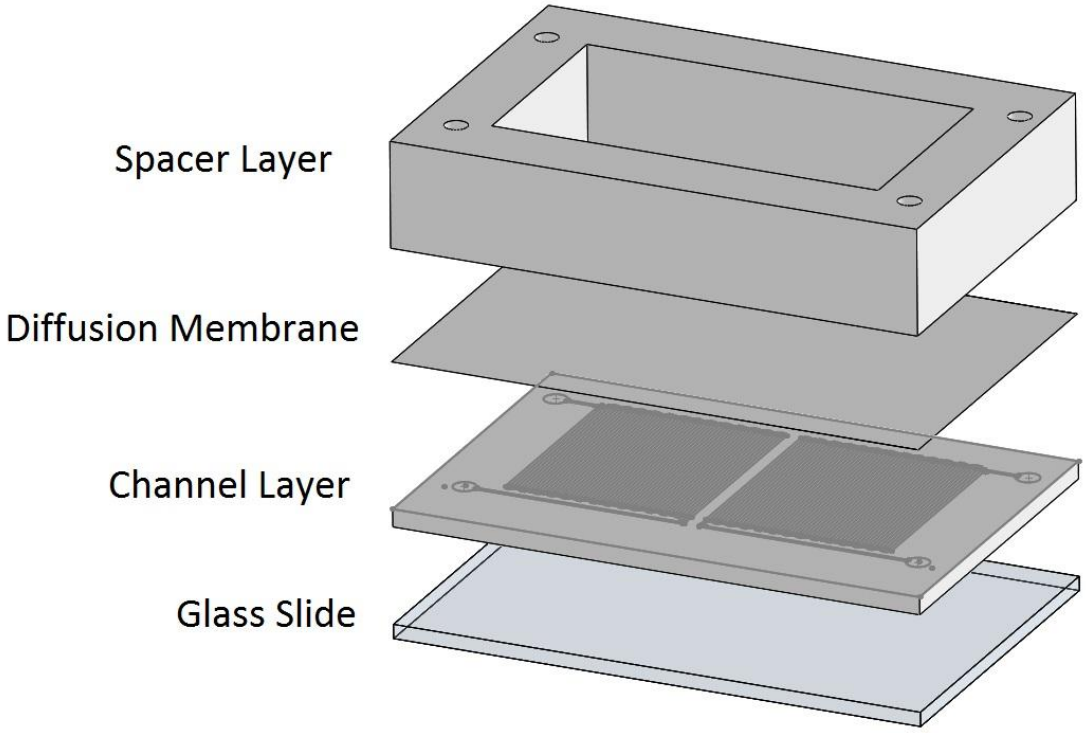

Figure 2.8. Exploded view schematic of the device construction. The channel layer was bonded to the glass slide, with the channel side facing up. It was then bonded to a 100μm thick diffusion membrane layer. Lastly, the approximately 2mm thick spacer layer was added to the very top in line with the inlet and outlet ports of the channel layer.

2.2 - Experimental set-up

2.2.1 - Oxygen fluorescence imaging

For both design iterations, the procedure for oxygen fluorescence imaging is almost exactly the same. The only difference came in the gradient measurements taken at different time points for the open well channel devices. In order to examine the oxygen flow profiles of the microfluidic devices, a fluorescent microscope was used in conjunction with the MetaMorph® software. For this experiment, different combinations of 0% and 21% O_2 are pumped through the device. The gas tanks are connected to the inlet ports using plastic connectors and Tygon tubing with a 1/16 inch inner diameter (ID) and 1/8 inch outer diameter (OD). Once the gas tanks are connected and the PtOPEK sensor is placed, the open well spacer layer is filled with 5 mL of deionized (DI) water.

The constructed device is placed on the microscope stage and each inlet port is connected to the gas tanks. A schematic of the set-up is shown in Figure 2.9. The microscope images are taken at 4X magnification.

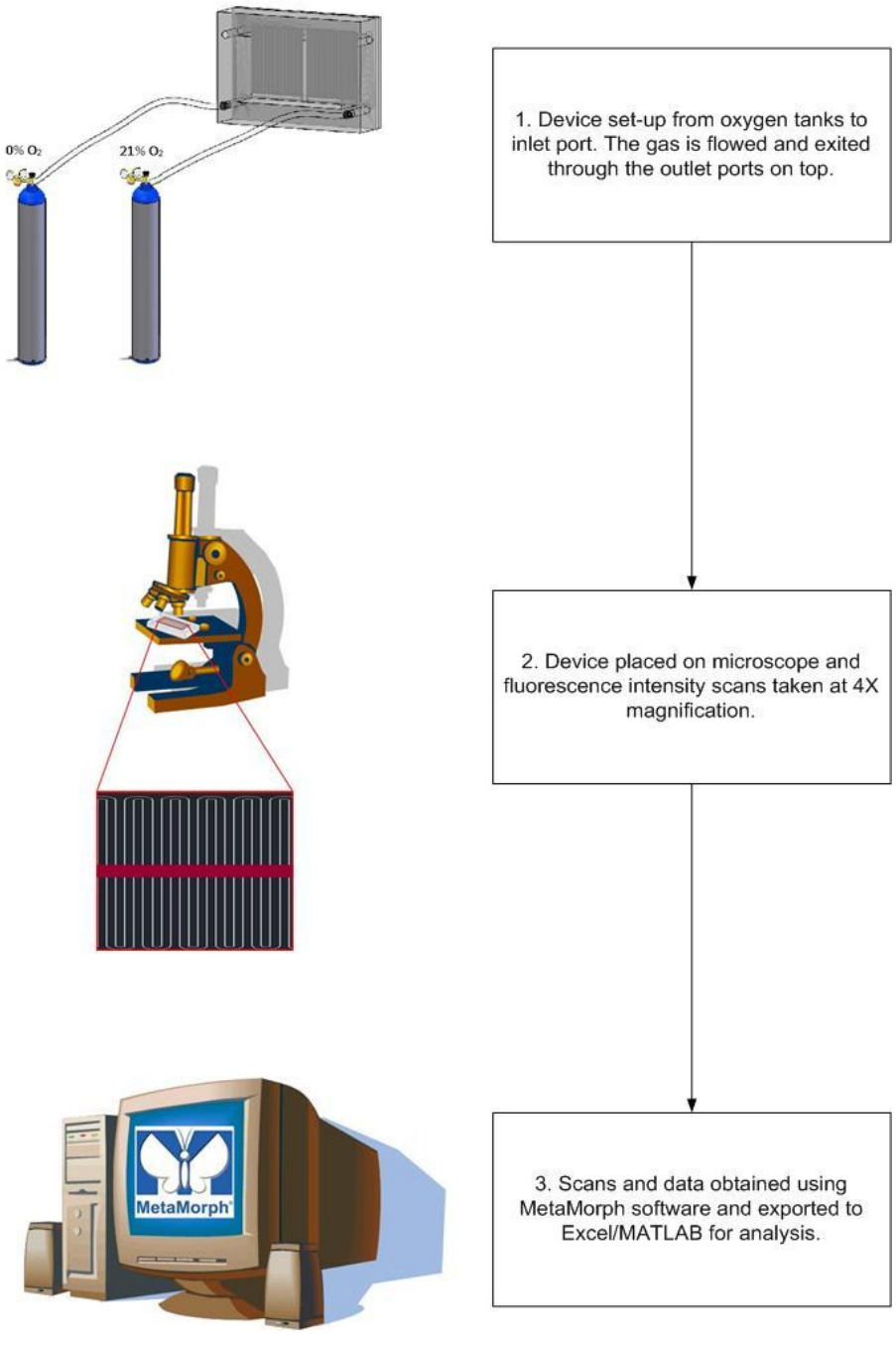

Figure 2.9. Experimental set-up. The device is connected to oxygen tanks via the inlet ports, and the gas is allowed to flow out through the outlet port. The device is placed on the microscope stage and images are taken at 4X magnification using the MetaMorph software. The linescan data containing the fluorescence intensity values are exported to Excel and then processed in MATLAB for analysis.

For calibration, images were taken when the inlet channels were both connected to 0% and then to 21% O_2, pumped at 30 mL/min as measured by a flow rotometer. Using the MetaMorph® Premier software, the slide area was defined where the sensor was placed and the slide was scanned 5 times at each measurement to reduce the presence of any outlier data. When switching from 0% to 21% O_2 for calibration, the device was allowed to equilibrate at the present state for approximately 10 minutes. To observe the dual condition, the left side of the device was pumped with 30 mL/min of 0% O_2 while the right side of the device was pumped with 30 mL/min of 21% O_2, ensuring that the sensor covered both regions of the device. The dual condition was allowed to equilibrate for approximately 30-45 minutes in the serpentine channel devices, and the slide was scanned 5 times at the dual condition setting. The data for the open-well devices were obtained the same way. However, a time-lapse experiment was also performed for the open-well devices to examine the length of time for equilibration. The dual condition for the gradient measurements were taken at different time points for a total of 15 readings ranging from immediately after the gas was connected to about 70 minutes after connection, with scans taken every 5 minutes. Once the scans were obtained, a linescan of the same region was performed on each of the slide scans for all three conditions tested to quantify the fluorescence pixel intensity readings for each. This data was exported to Excel for further processing and analysis.

2.3 - Data analysis

2.3.1 - Stern-Volmer and triangle smoothing

Each exported Excel file contained data for the three conditions: 0% O_2, 21% O_2, and the dual condition. The average of the five intensity values was calculated, reducing skewed data resulting from the presence of outliers. The data was entered into a new spreadsheet with the

(X,Y) position coordinates and the averaged intensity values. Sheet 1 contained the average of the 0% O_2 data, Sheet 2 contained the average of the 21% O_2 data, and Sheet 3 contained the average of the dual condition data. The Stern-Volmer equation was used to calculate the oxygen percentages based on the given intensity values as shown in Equation 2.3:

$$\frac{I_0}{I} = 1 + K_q[O_2] \tag{2.3}$$

where I is the fluorescence intensity, I_0 is the fluorescence intensity without oxygen, and K_q is the quenching constant(41). The Stern-Volmer equation was used through a MATLAB function and the oxygen percentage data was exported to an Excel file and examined using a scatter plot. Many of the oxygen percentage data showed outliers and noise that affected the way the data was represented which could affect the calculation of the gradient slope. To reduce the amount of noise in the oxygen percentage data, the data was run through MATLAB in a triangle smoothing function provided in Appendix A to create a bandpass filter to create a smoothed curve of oxygen percentage data, though the trends of the curves remained the same. The smoothed data was used by choosing a triangle window of L = 81 for optimal smoothing. This data was again exported to a new Excel spreadsheet and examined using a scatter plot.

2.3.2 - Gradient slope calculation//visualization

The oxygen percentage data was represented in a scatter plot and examined manually. The last value of the lower plateau was taken and the first value of the upper plateau was taken to examine the slope of the gradient observed. Because of outlier and different data noise, the calculation for the slope was difficult to perform consistently across each data set for all the

different parameters. As such, the graphs for each trial were put together for visual examination for each parameter of interest, and then altogether in one graph. This visualization allowed for a more consistent and thorough observation across data sets and a clearer view of the oxygen gradient slope profile trends.

CHAPTER III: RESULTS

3.1 Serpentine channel

3.1.1 Channel span

One of the first parameters examined was the span of the device. As previously defined, the span of the device referred to the length of one of the serpentine channel loops, from top to bottom. The range of spans that were examined were 10mm, 20mm, 30mm, and 40mm. In addition to the span, the depth of the channel which is determined by the thickness of the SU-8 photoresist spun on the master, was examined. The standard 140μm depth was compared to a deeper 265μm master depth. The oxygen percentage plots for channel span 10mm, 20mm/30mm, and 40mm with their respective depths are shown in Figure 3.1. A combined plot for all the span devices with differing depths is also shown in Figure 3.1 to show that there was no significant difference in the oxygen gradient slope profiles for this examined parameter.

Figure 3.1. Serpentine channel span plots. A) Plots for the 10mm span devices at both 140μm depth channels and 265μm channels. B) Plots for the 20mm and 30mm span devices at 140μm

depth channels. C) Plots for the 40mm span devices at both 140µm depth channels and 265µm channels. D) Combined plot for the span devices.

A)

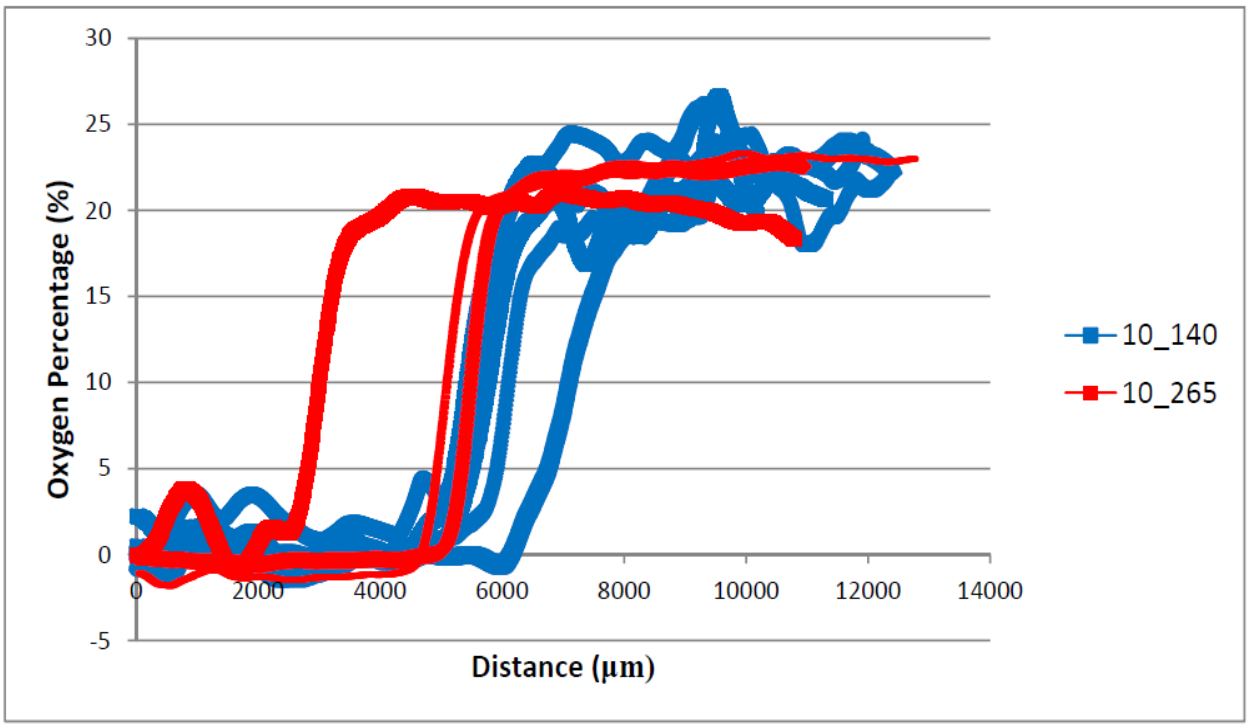

B)

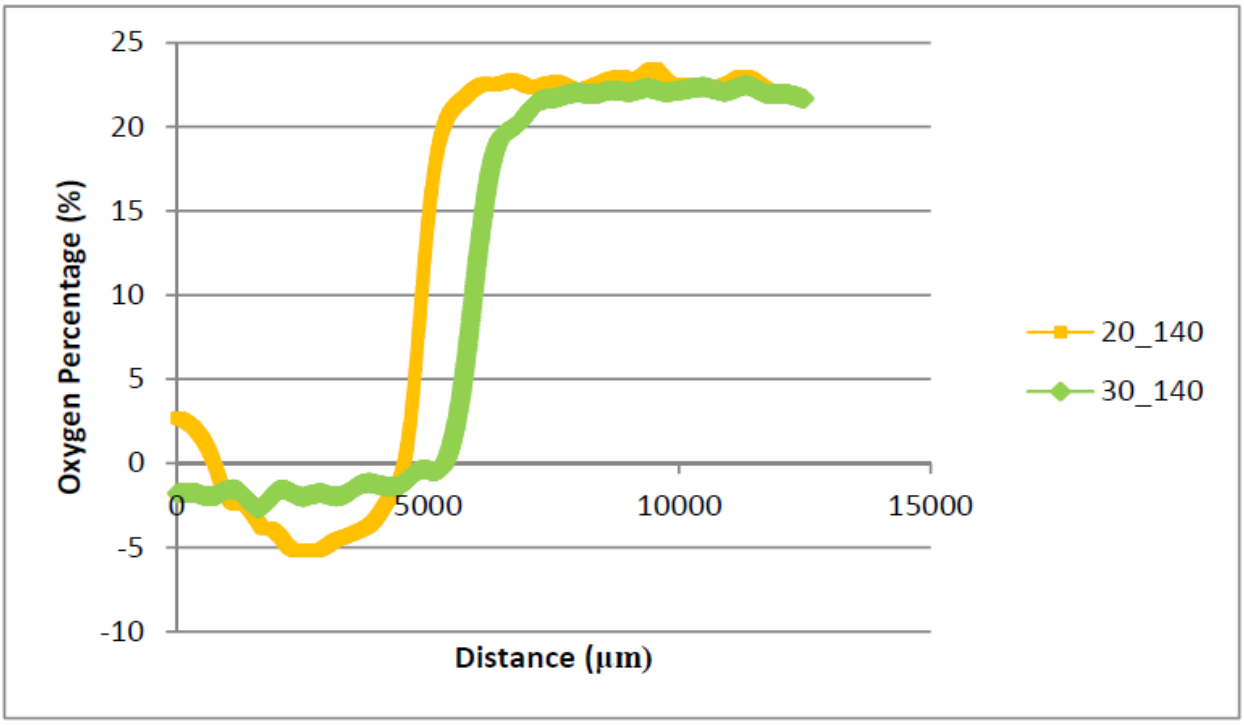

C)

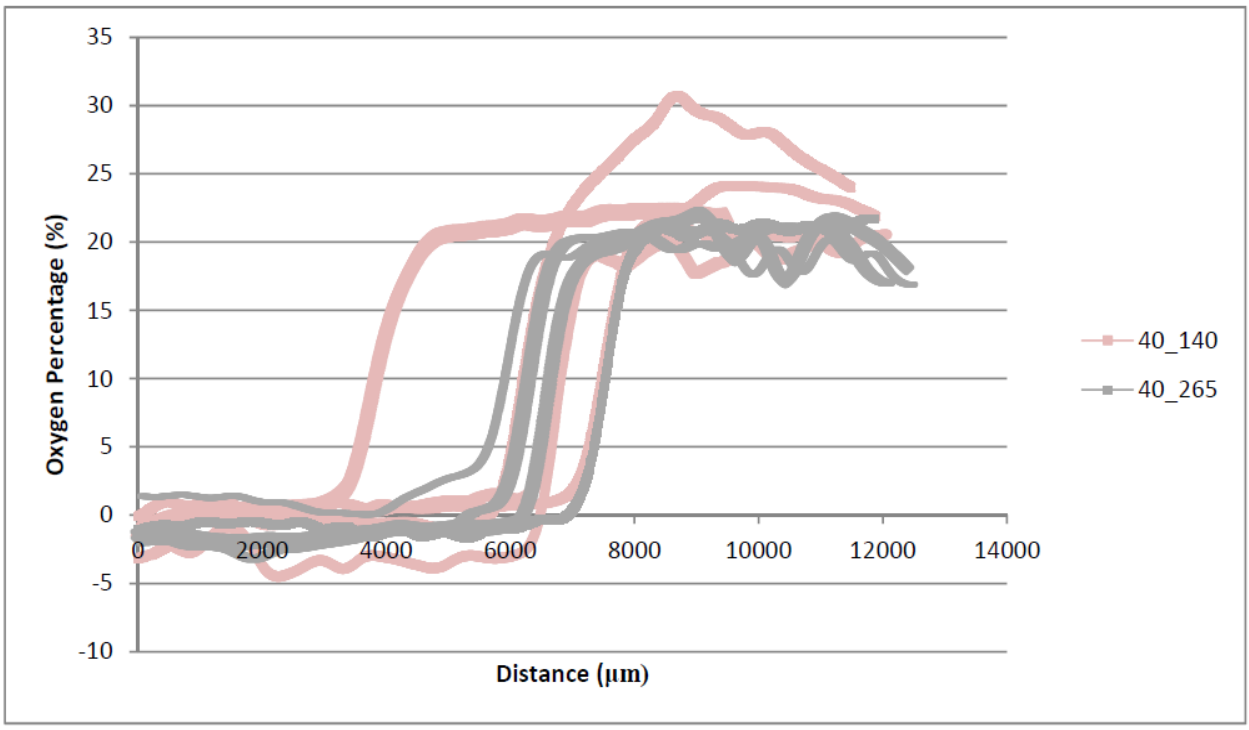
35
30
25
20
15
10
5
0
-5
-10
Oxygen Percentage (%)
0
2000
4000
6000
8000
10000
12000
14000
Distance (µm)
40_140
40_265

D)

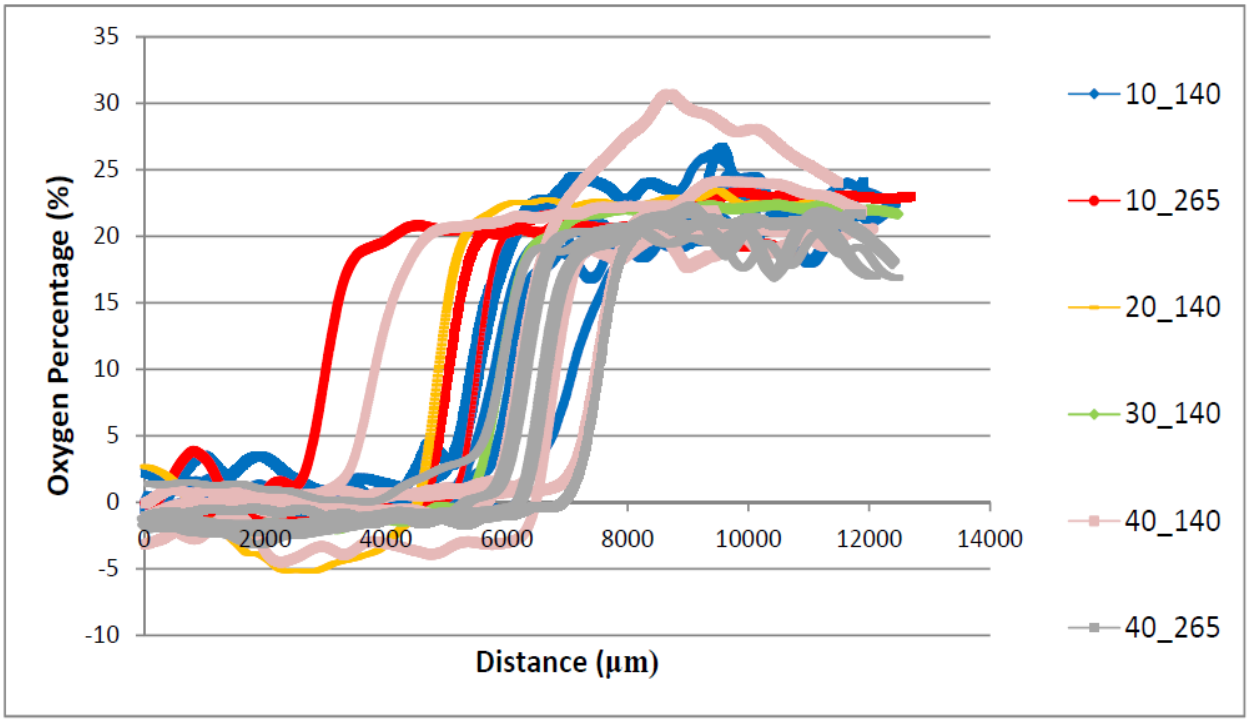
35
30
25
20
15
10
5
0
-5
-10
Oxygen Percentage (%)
0
2000
4000
6000
8000
10000
12000
14000
Distance (µm)
10_140
10_265
20_140
30_140
40_140
40_265

3.1.2 Channel layer thickness

The thickness of the PDMS poured onto the channel layer was expected not to make a significant difference on the results, since the amount of PDMS did not actually change any structural function. To test this hypothesis, different amounts of PDMS were poured to create channel layers of varying thicknesses. The thicknesses observed were 1mm, 2mm, and 4mm poured onto the 30mm span serpentine channel device. The results observed from these differing PDMS thickness devices of 1mm, 2mm, and 4mm are shown in Figure 3.2. Based on these results, it seems that the 4x magnification on the microscope cannot give consistent readings on the 4mm thick devices, creating an upper threshold for thickness of the device. A combined plot is also shown in Figure 3.2 to show that there is no significant difference in the amount of PDMS poured onto the channel layer, as expected.

Figure 3.2. Serpentine PDMS thickness plots. A) Plot for 1mm thick PDMS channel layer devices. B) Plot for 2mm thick PDMS channel layer devices. C) Plot for 4mm thick PDMS channel layer devices. D) Combined plot for PDMS thickness channel layer devices.

A)

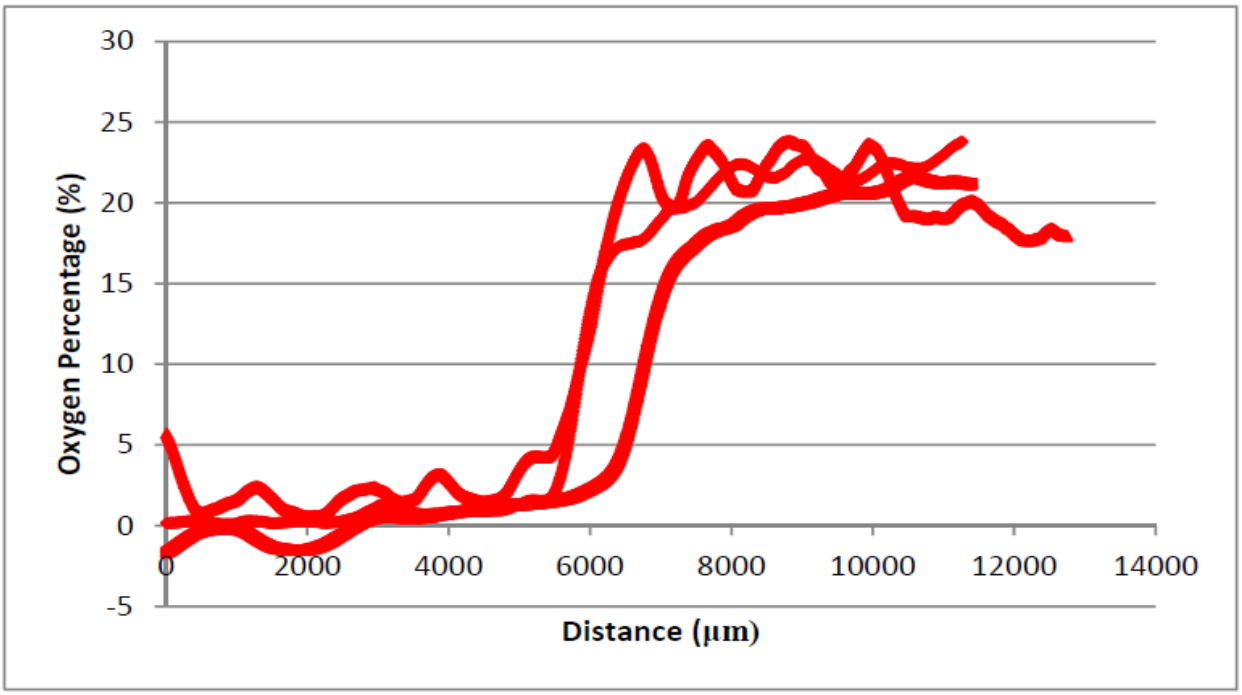
30
25
20
15
10
5
0
-5
Oxygen Percentage (%)
0
2000
4000
6000
8000
10000
12000
14000
Distance (µm)

B)

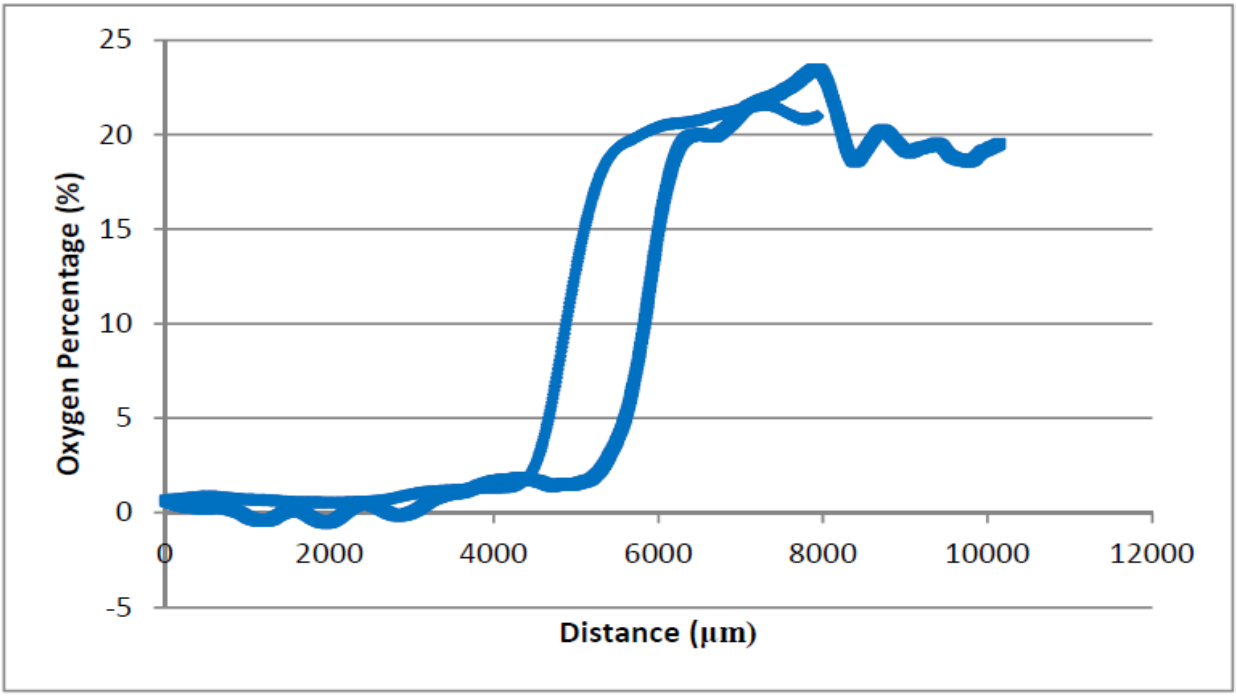
25
20
15
10
5
0
-5
Oxygen Percentage (%)
0
2000
4000
6000
8000
10000
12000
Distance (µm)

C)

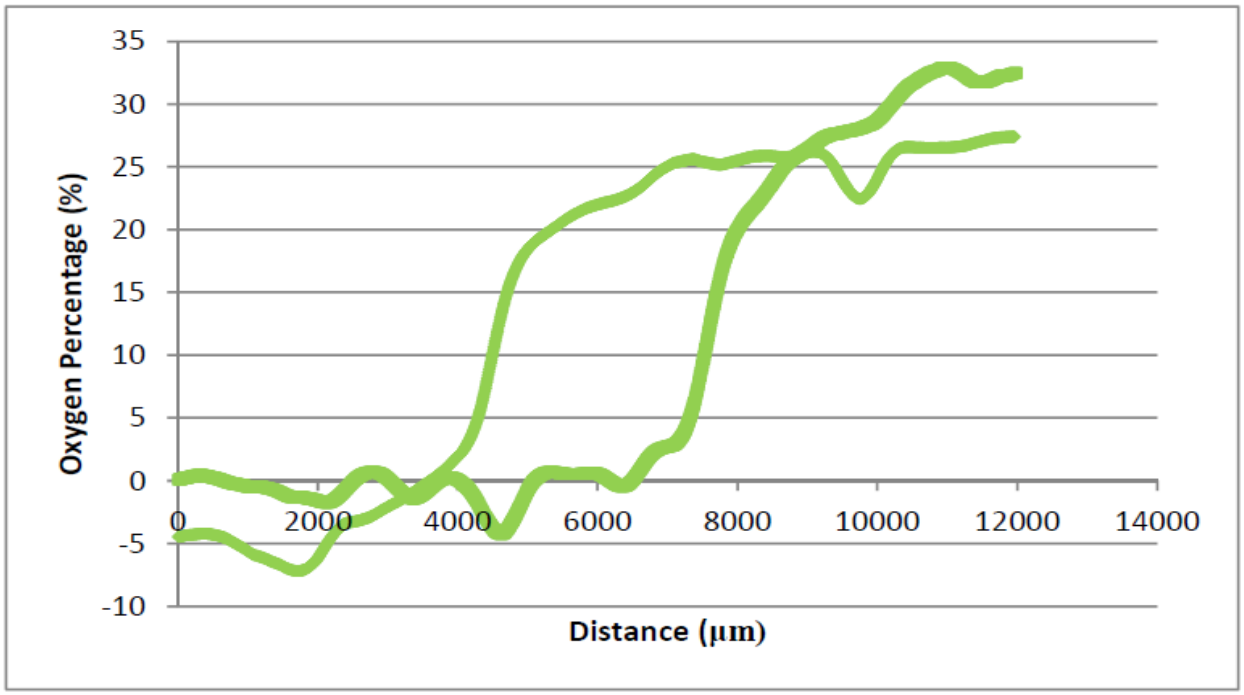
35
30
25
20
15
10
5
0
-5
-10
Oxygen Percentage (%)
0
2000
4000
6000
8000
10000
12000
14000
Distance (µm)

D)

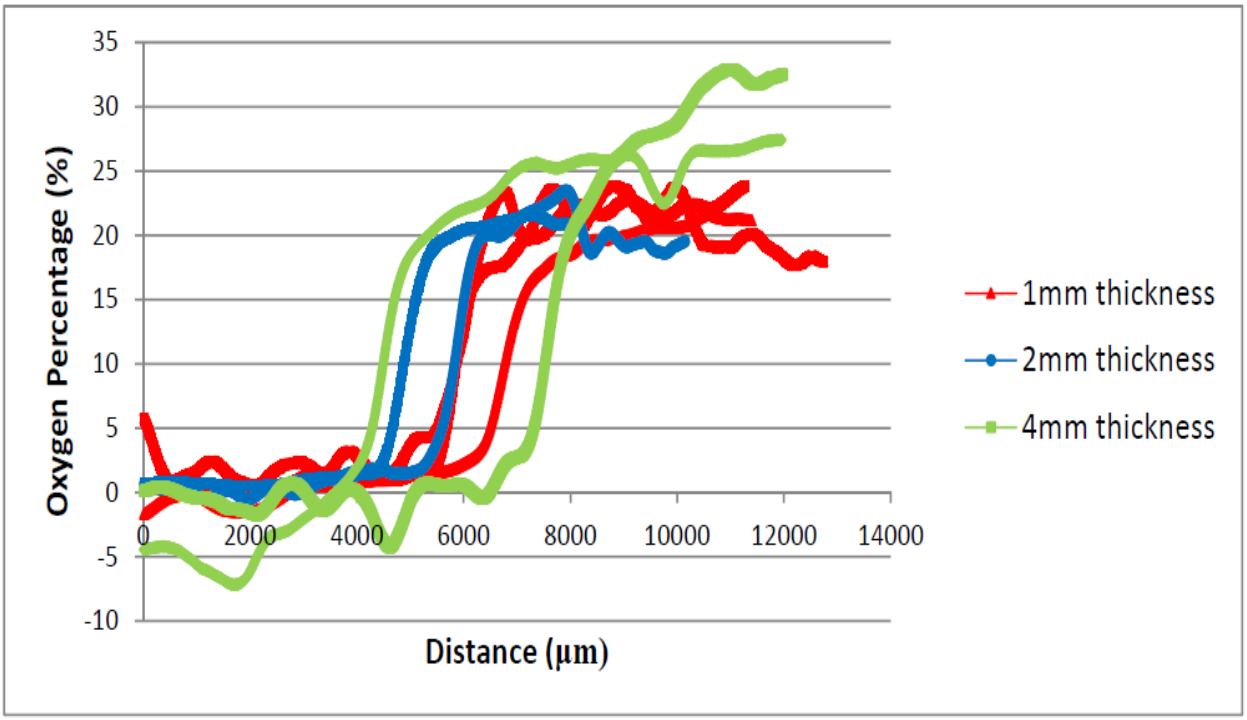
35
30
25
20
15
10
5
0
-5
-10
Oxygen Percentage (%)
0
2000
4000
6000
8000
10000
12000
14000
Distance (µm)
1mm thickness
2mm thickness
4mm thickness

3.1.3 Channel gap spacing

Because the designed device was a dual condition device, it was hypothesized that the spacing between the hypoxic (0%) and normoxic (21%) channels would play a significant role in the oxygen gradient slope profile. Since the two chambers examined were identical, the resistances would be the same across the device, but the space between the chambers was expected to show differing results in the oxygen gradient profile. The further apart the two channel conditions were, it was anticipated that the oxygen gradient profile would be smaller and a more gradual shift because of the greater distance that the gas needed to diffuse to create a gradient. The spacings examined between the two channel conditions were 0.250mm, 1mm, and 2mm. The results observed from the 0.250mm, 1mm, and 2mm spacing devices are displayed in Figure 3.3. A combined plot for the different spacing parameters is also shown in Figure 3.3 to show that there was no significant difference found in the oxygen gradient slope profile for the spacing parameter, though there seemed to be a more significant difference than the other parameters. This result led to the spacing parameter to be the only parameter of interest in the modified design of the open well chamber device.

Figure 3.3. Serpentine gap spacing plots. A) Plot for 0.250mm gap spacing devices. B) Plot for 1mm gap spacing devices. C) Plot for 2mm gap spacing devices. D) Combined plot for all gap spacing serpentine channel devices.

A)

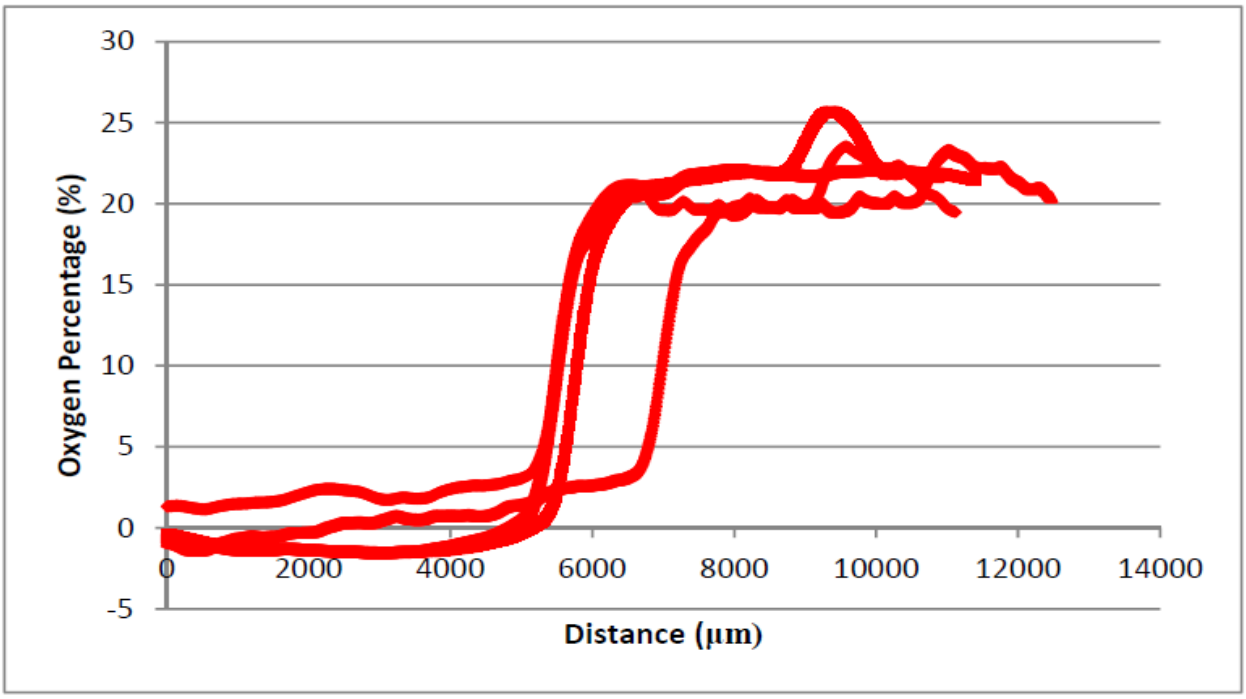
30
25
20
15
10
5
0
-5
Oxygen Percentage (%)
0
2000
4000
6000
8000
10000
12000
14000
Distance (µm)

B)

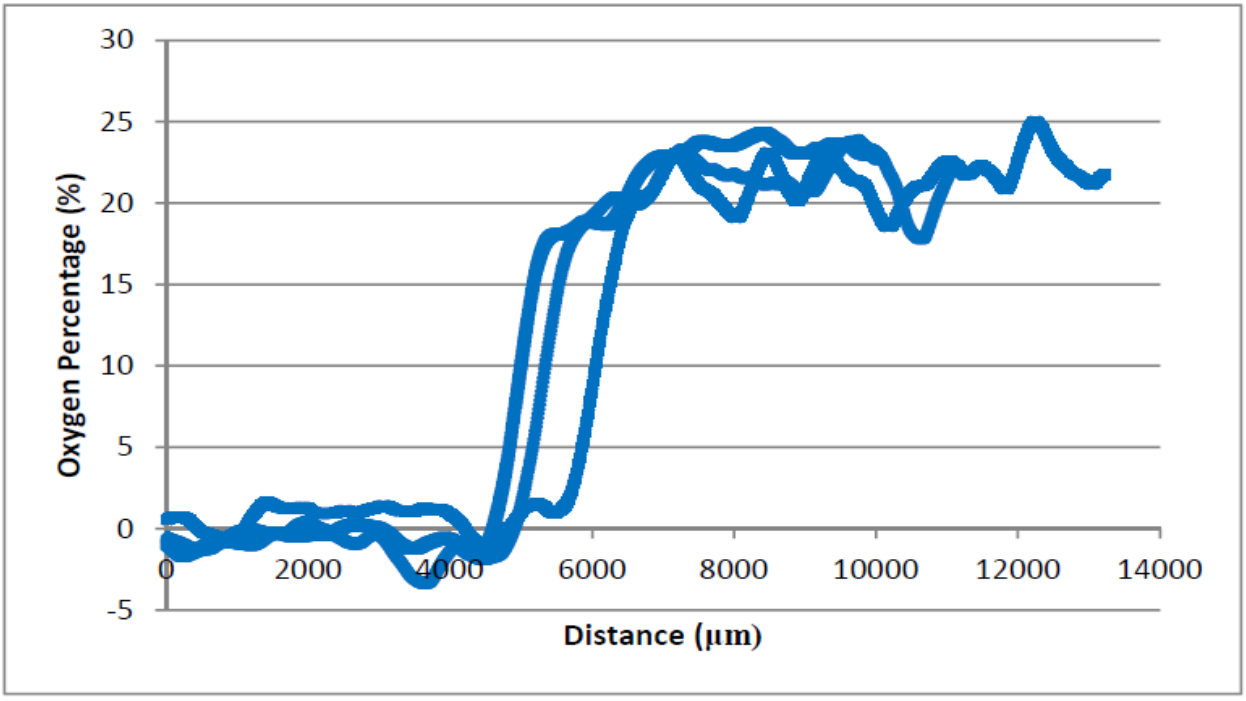
30
25
20
15
10
5
0
-5
Oxygen Percentage (%)
0
2000
4000
6000
8000
10000
12000
14000
Distance (µm)

C)

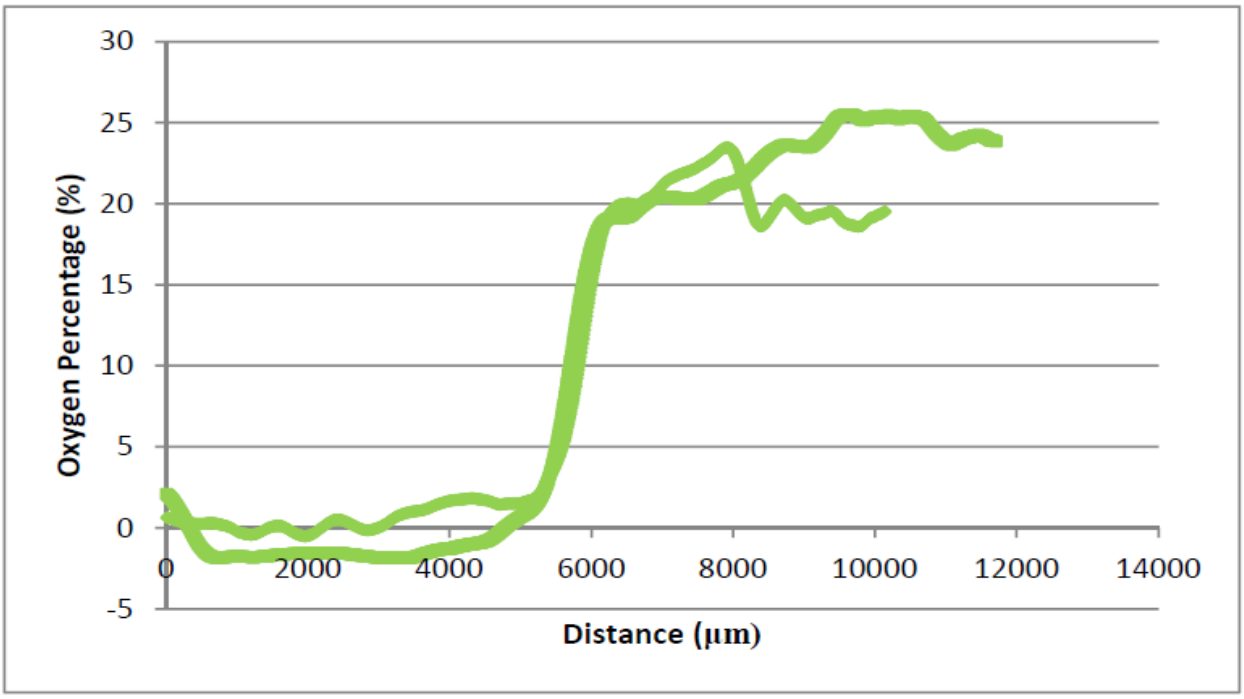
30
25
20
15
10
5
0
-5
Oxygen Percentage (%)
0
2000
4000
6000
8000
10000
12000
14000
Distance (µm)

D)

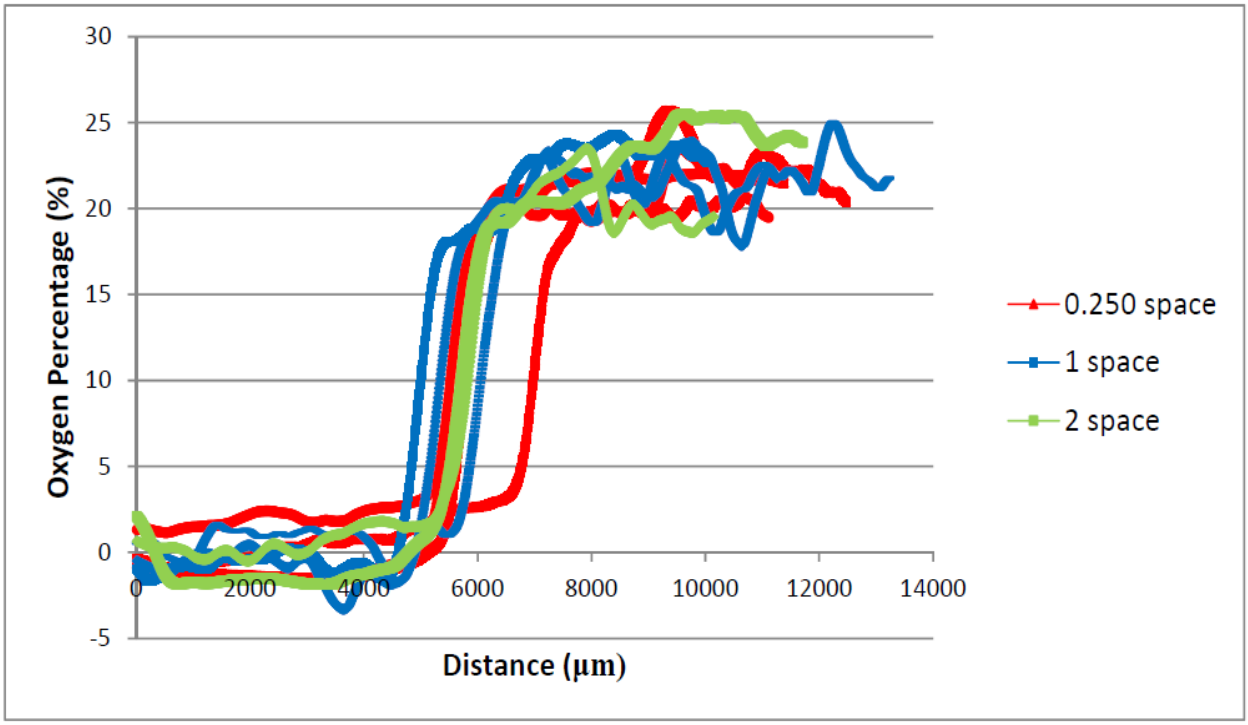
30
25
20
15
10
5
0
-5
Oxygen Percentage (%)
0
2000
4000
6000
8000
10000
12000
14000
Distance (µm)
0.250 space
1 space
2 space

3.1.4 Channel width

The width of the channel designs was thought to play a significant role in the gradient slope profile because a larger channel would lead to substantially decreased resistance in the channels. The channel widths observed were 0.075mm, 0.250mm, and 0.750mm. It was expected that there would be a substantial difference between the thinnest and the thickest channel widths of 0.075mm and 0.750mm, respectively. The thick 0.750mm width channel device was expected to have a lower and more gradual oxygen gradient slope than the thinner channels because of a lower resistance in the device. The plots for the channel widths of 0.075mm, 0.250mm, and 0.750mm are shown in Figure 3.4. A combined plot is also shown in Figure 3.4 to show that there is no significant difference in the gradient slope values from the differing channel widths.

Figure 3.4. Serpentine channel width plots. A) Plot for 0.075mm channel width devices. B) Plot for 0.250mm channel width devices. C) Plot for 0.750mm channel width devices. D) Combined plot for all serpentine channel width devices.

A)

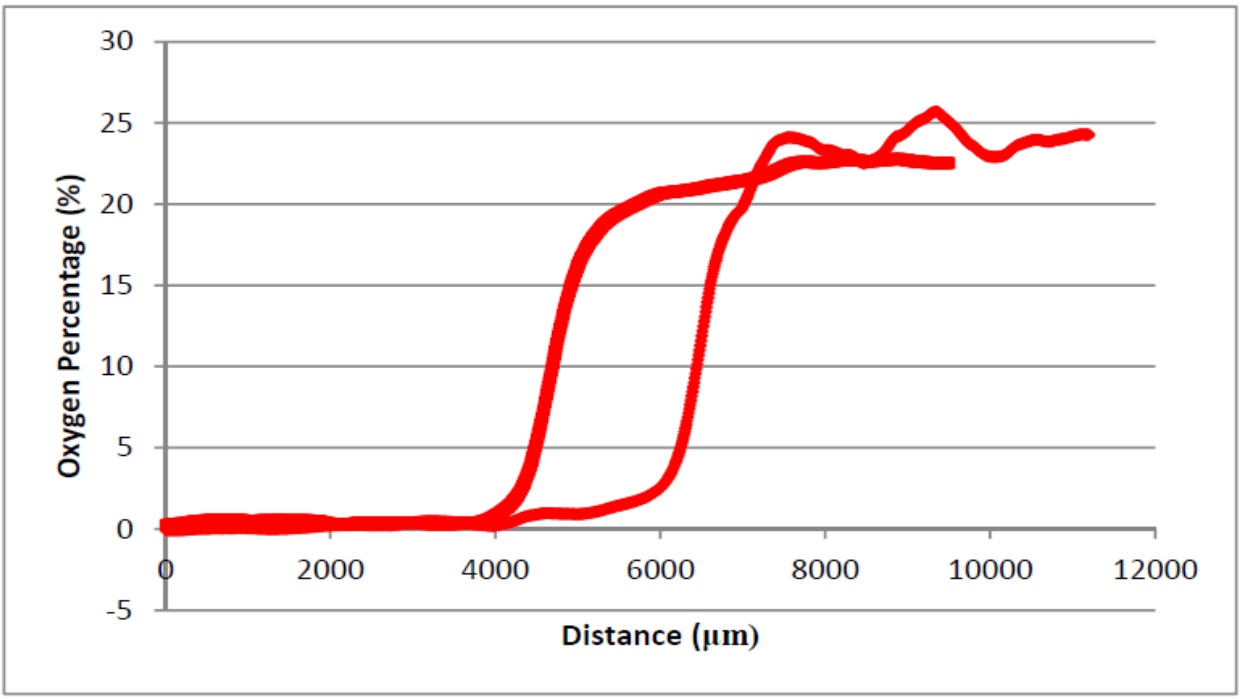
30
25
20
15
10
5
0
-5
Oxygen Percentage (%)
0
2000
4000
6000
8000
10000
12000
Distance (µm)

B)

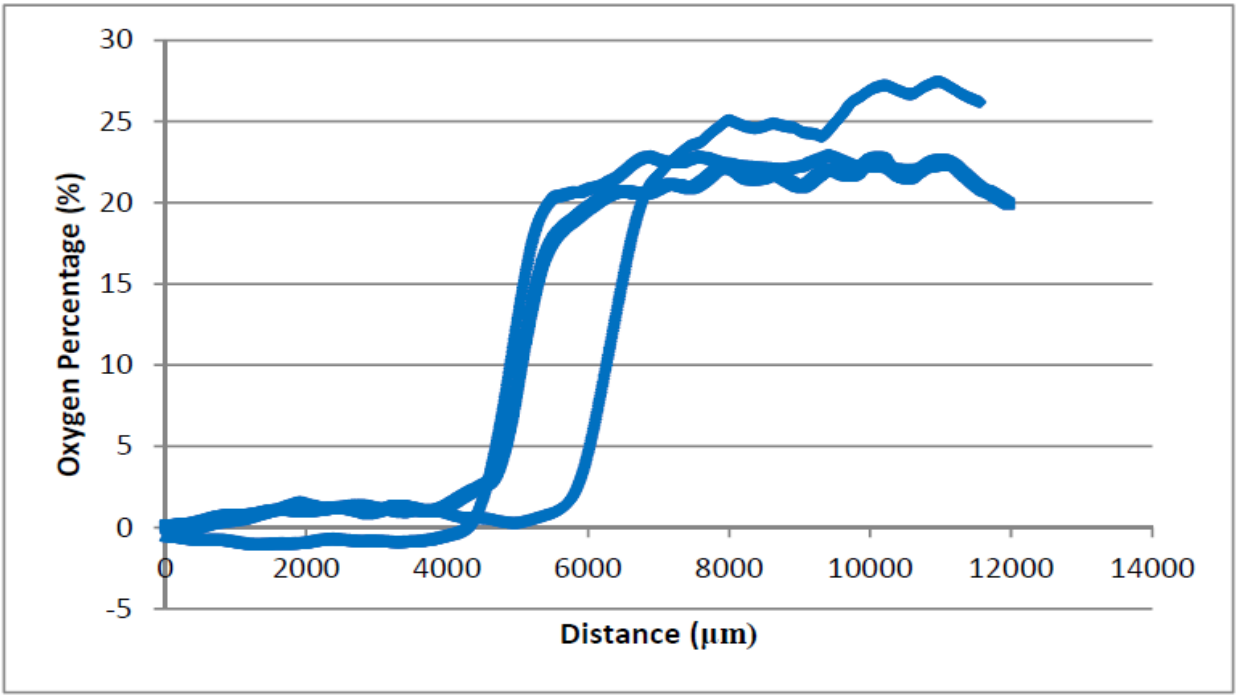
30
25
20
15
10
5
0
-5
Oxygen Percentage (%)
0
2000
4000
6000
8000
10000
12000
14000
Distance (µm)

C)

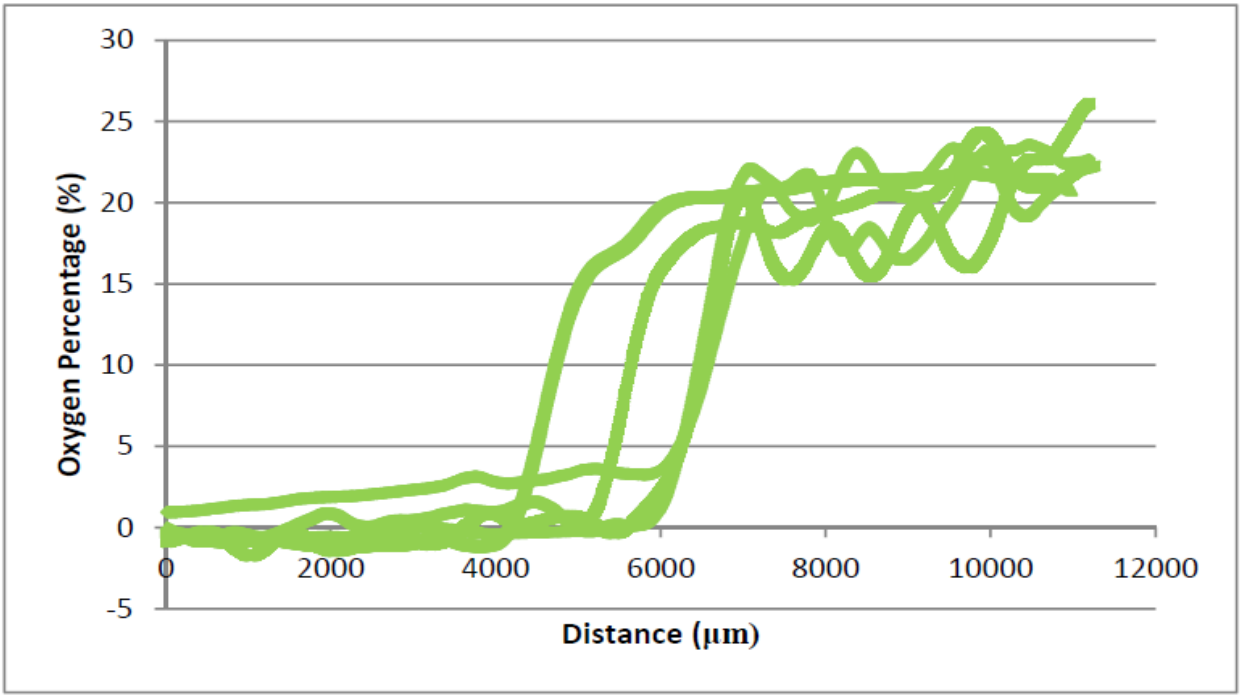
30
25
20
15
10
5
0
-5
Oxygen Percentage (%)
0
2000
4000
6000
8000
10000
12000
Distance (µm)

D)

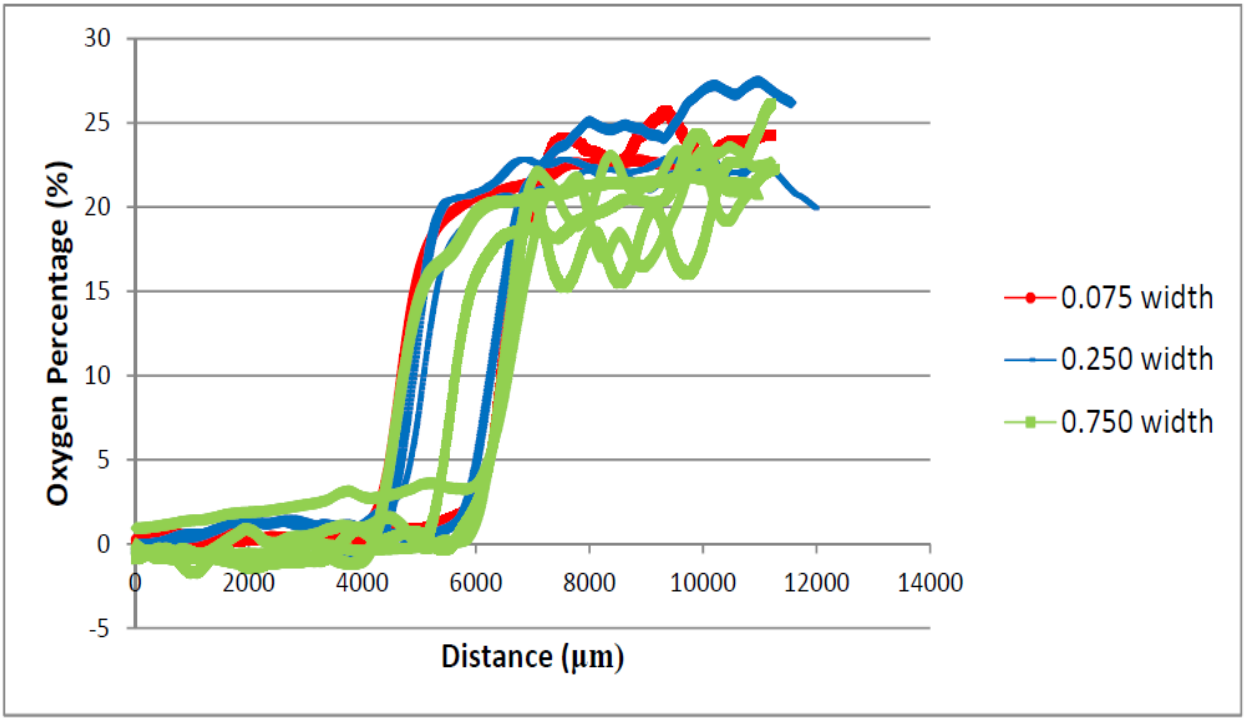
30
25
20
15
10
5
0
-5
Oxygen Percentage (%)
0
2000
4000
6000
8000
10000
12000
14000
Distance (µm)
0.075 width
0.250 width
0.750 width

3.2 Open-well channel

3.2.1 Channel gap spacing

Based on the results from the serpentine channel devices, the gap spacing seemed to have the biggest effect on the gradient slope profiles. The gap spacing parameter was also considered because of its identical resistance values in the hypoxic and normoxic chambers. It was hypothesized that a significant difference could not be observed in the initial experiments because of the high resistance in the channels from the serpentine channel design. Based on this assumption, the open-well channel design was tested to isolate and examine the effect of a 0.250mm and 2mm gap spacing, as tested in the serpentine channels, on the low resistance open-well channel designs described previously. The flows used in the serpentine channel devices of 30mL/min were kept constant in the testing of the open-well channel designs. The results for the 0.250mm and 2mm gap spacing open-well channels are shown in Figure 3.5. Surprisingly, the plot for the combined graph, also shown in Figure 3.5 showed that there was again no significant difference in the gap spacings in the low resistance open-well channel designs.

Figure 3.5. Open-well channel gap spacing devices. A) Plots for 0.250mm spacing open-well devices. B) Plots for 2mm spacing open-well devices. C) Combined plot for open-well gap spacing devices.

A)

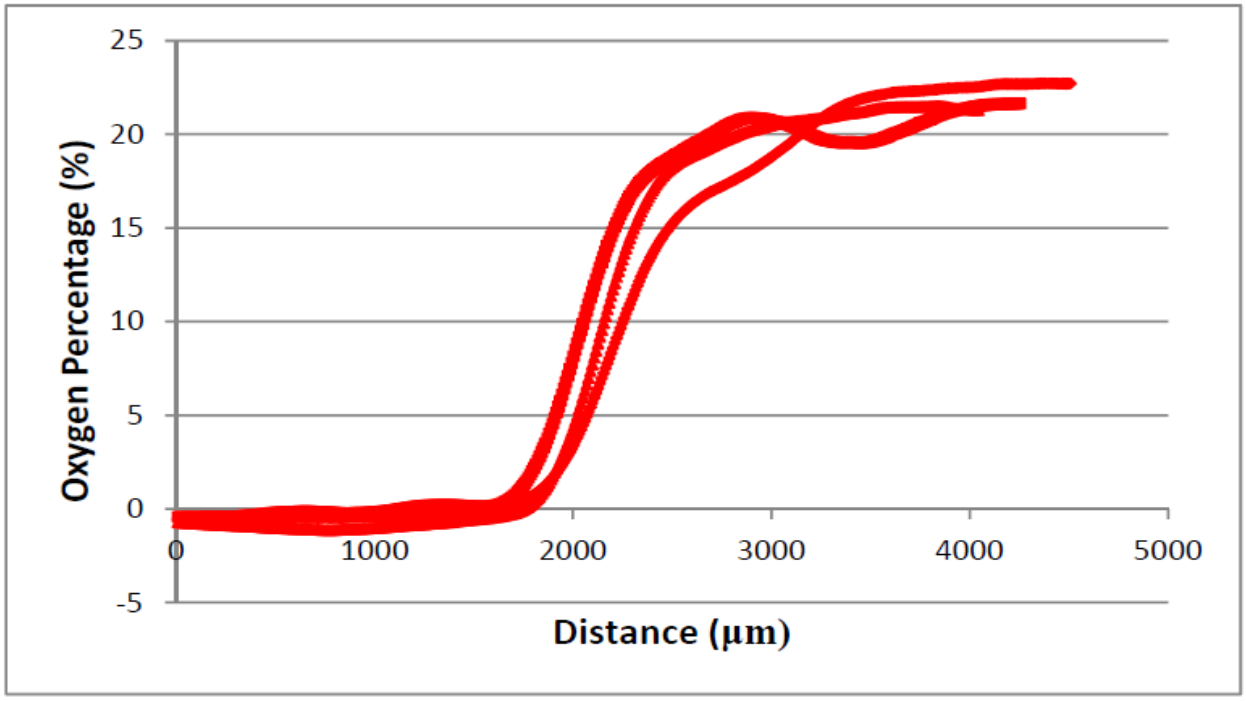
25
20
15
10
5
0
-5
Oxygen Percentage (%)
0
1000
2000
3000
4000
5000
Distance (µm)

B)

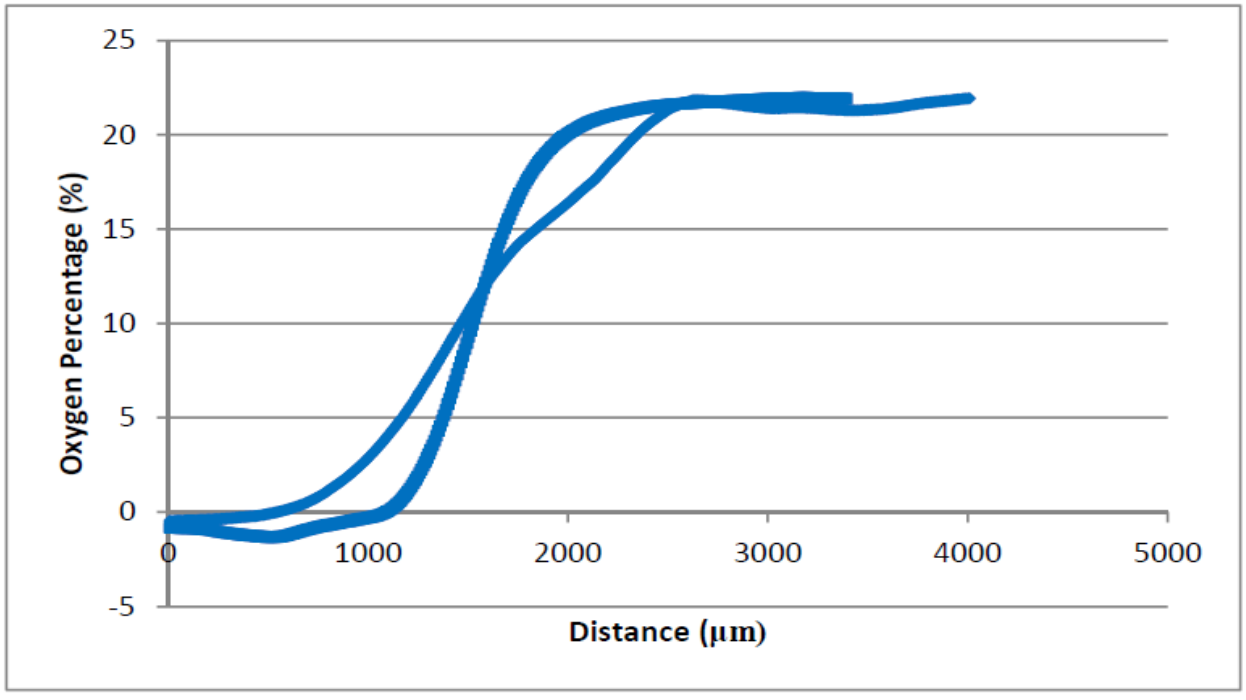
25
20
15
10
5
0
-5
Oxygen Percentage (%)
0
1000
2000
3000
4000
5000
Distance (µm)

C)

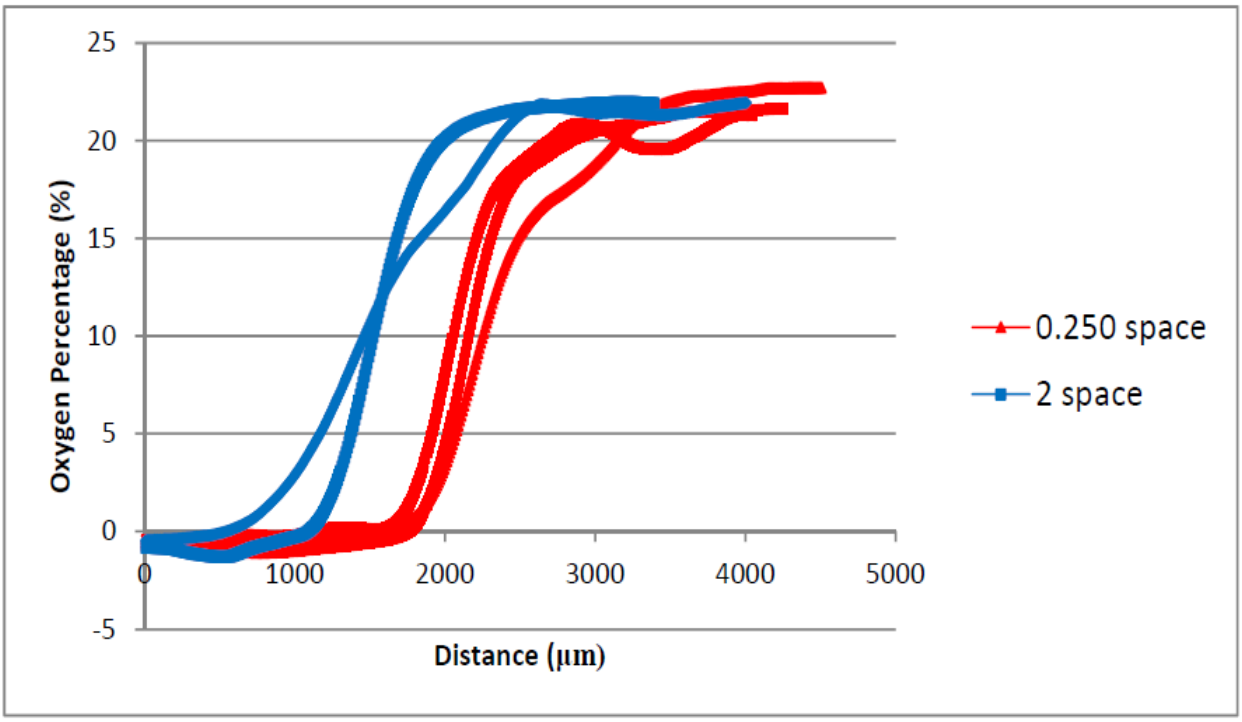

3.2.2 Time-lapse

An additional possible explanation explored for the identical gradient slope profiles examined was the effect of the length of time that the device was allowed to equilibrate at the dual condition. The hypothesis was that the 40-50 minutes that the device was allowed to equilibrate at the dual condition allowed for the gas to diffuse into the gap, creating a profile that was identical to a dual condition device that had almost no spacing at all. As such, a time-lapse of the dual condition was performed to examine whether or not the diffusion of gas showed significant differences in the oxygen slope profile based on the length of time that the device was allowed to equilibrate. The device was scanned every 5 minutes, with the first scan being immediately after connection (0 minutes) and the last scan being approximately 70 minutes after connection to the

dual condition. The plots for the time-lapse on both the 0.250mm and 2mm gap spacing open-well channel devices are shown in Figure 3.6. When compiled together as also shown in Figure 3.6, it was again surprising to examine that the device equilibrated rather quickly (between 3 and 5 minutes), and showed the same gradient slope profiles, regardless of the time and spacing.

Figure 3.6. Open-well channel time lapse plots. A) Plots for 0.250mm space open-well channel over 70 minutes. B) Plots for 2mm space open-well channel over 70 minutes. C) Combined plot for open-well devices over a time course of 70 minutes at 5 minute intervals.

A)

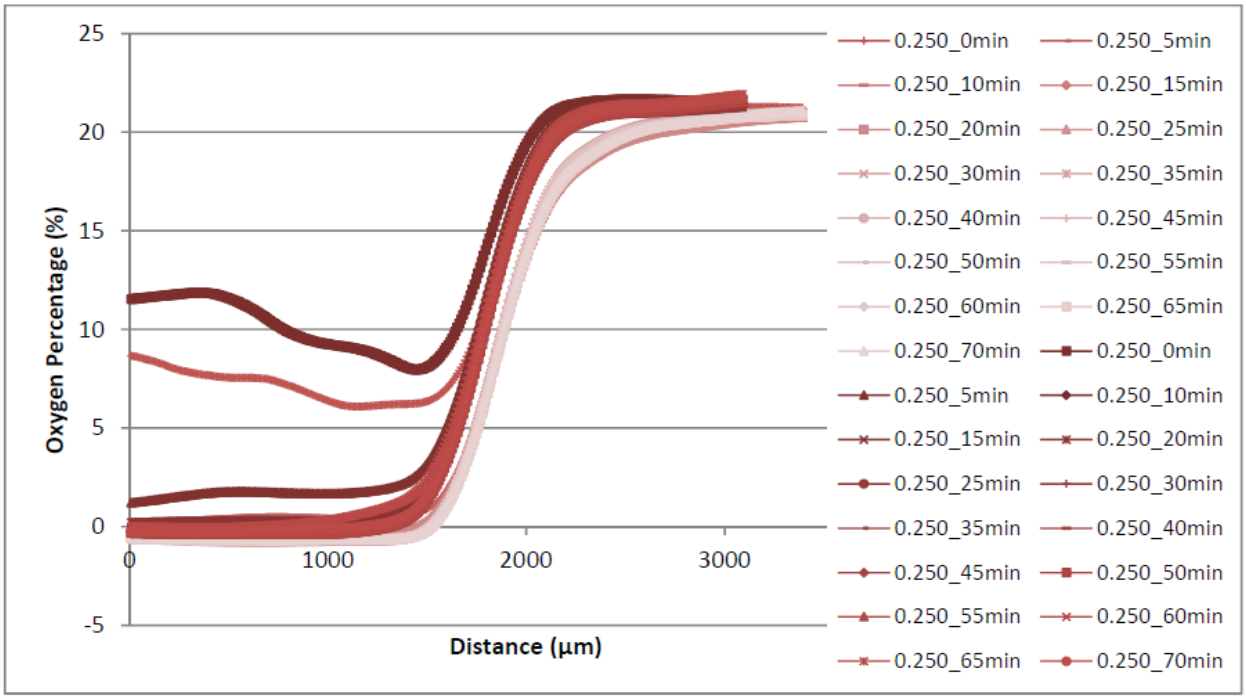
25
20
15
10
5
0
-5
0
1000
2000
3000
Oxygen Percentage (%)
Distance (µm)
0.250_0min
0.250_5min
0.250_10min
0.250_15min
0.250_20min
0.250_25min
0.250_30min
0.250_35min
0.250_40min
0.250_45min
0.250_50min
0.250_55min
0.250_60min
0.250_65min
0.250_70min
0.250_0min
0.250_5min
0.250_10min
0.250_15min
0.250_20min
0.250_25min
0.250_30min
0.250_35min
0.250_40min
0.250_45min
0.250_50min
0.250_55min
0.250_60min
0.250_65min
0.250_70min

B)

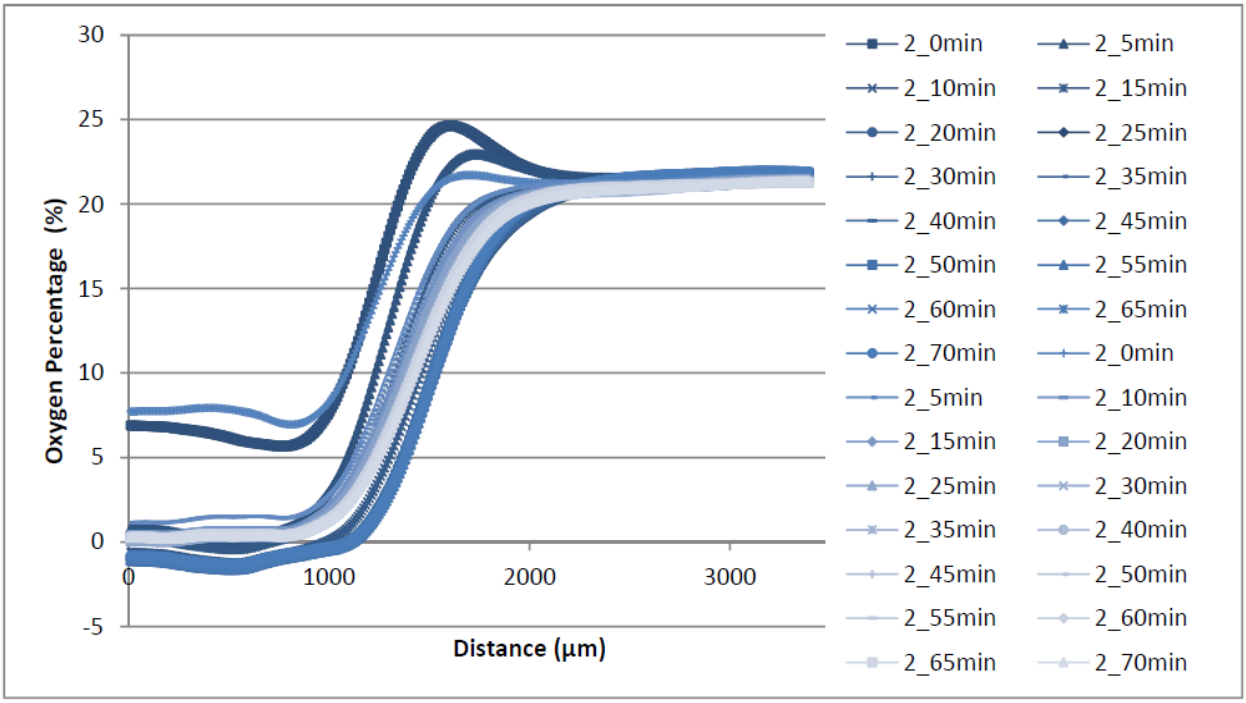
30
25
20
15
10
5
0
-5
0
1000
2000
3000
Oxygen Percentage (%)
Distance (µm)
2_0min
2_5min
2_10min
2_15min
2_20min
2_25min
2_30min
2_35min
2_40min
2_45min
2_50min
2_55min
2_60min
2_65min
2_70min
2_0min
2_5min
2_10min
2_15min
2_20min
2_25min
2_30min
2_35min
2_40min
2_45min
2_50min
2_55min
2_60min
2_65min
2_70min

C)

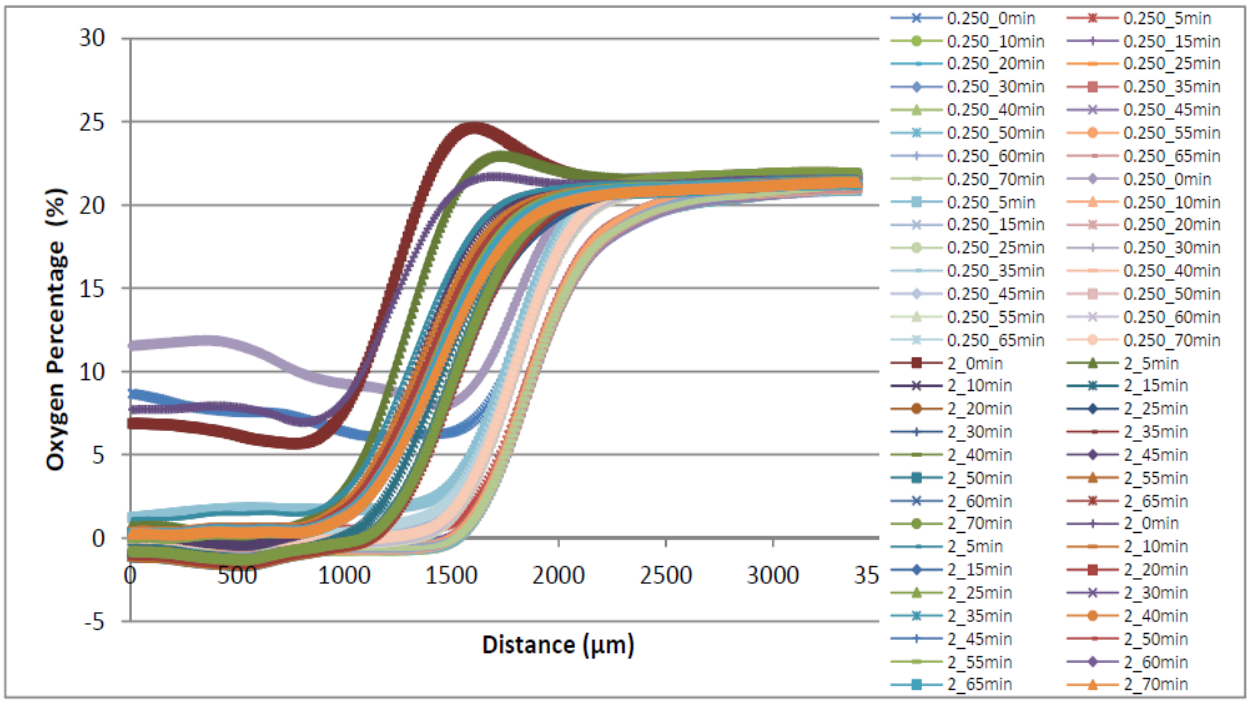

3.2.3 Slow-flow

A possible cause of the high resistance in the channels was hypothesized to be the speed of the gas that was flowed through the channels. To test this hypothesis and further reduce the resistance in the channels, experiments were run at a slow flow rate approximately 1/3 of the original 30mL/min rate. The gas was flowed at 10mL/min and the same procedure was repeated for the 0.250mm and 2mm spacing open-well devices. It was expected that this slower flow would give a significant difference in the gradient slope values. However, it was found that the slopes were relatively the same as shown in the plots for the 0.250mm and 2mm spacing in Figure 3.7. The combined plot, also shown in Figure 3.7, reiterates that there seems to be no significant difference in the incidence of the gradient slope values, even with the slower flow.

A)

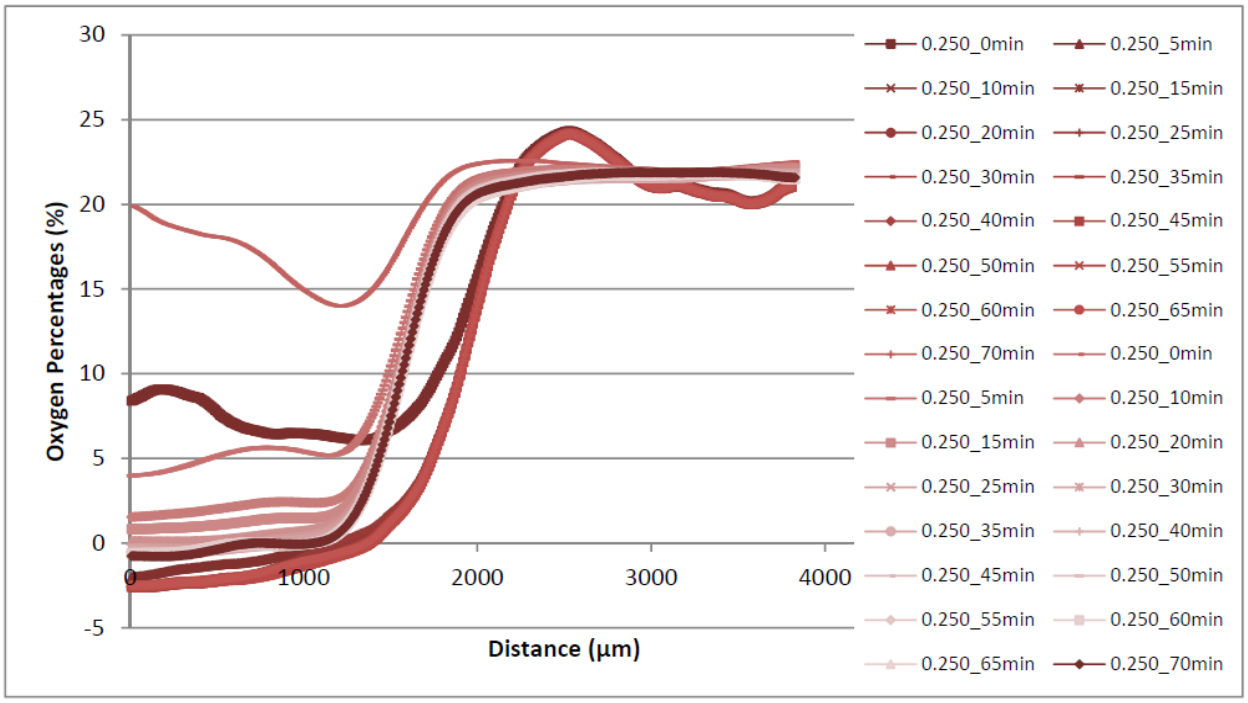
Oxygen Percentages (%)
30
25
20
15
10
5
0
-5
0
1000
2000
3000
4000
Distance (µm)
0.250_0min
0.250_5min
0.250_10min
0.250_15min
0.250_20min
0.250_25min
0.250_30min
0.250_35min
0.250_40min
0.250_45min
0.250_50min
0.250_55min
0.250_60min
0.250_65min
0.250_70min
0.250_0min
0.250_5min
0.250_10min
0.250_15min
0.250_20min
0.250_25min
0.250_30min
0.250_35min
0.250_40min
0.250_45min
0.250_50min
0.250_55min
0.250_60min
0.250_65min
0.250_70min

B)

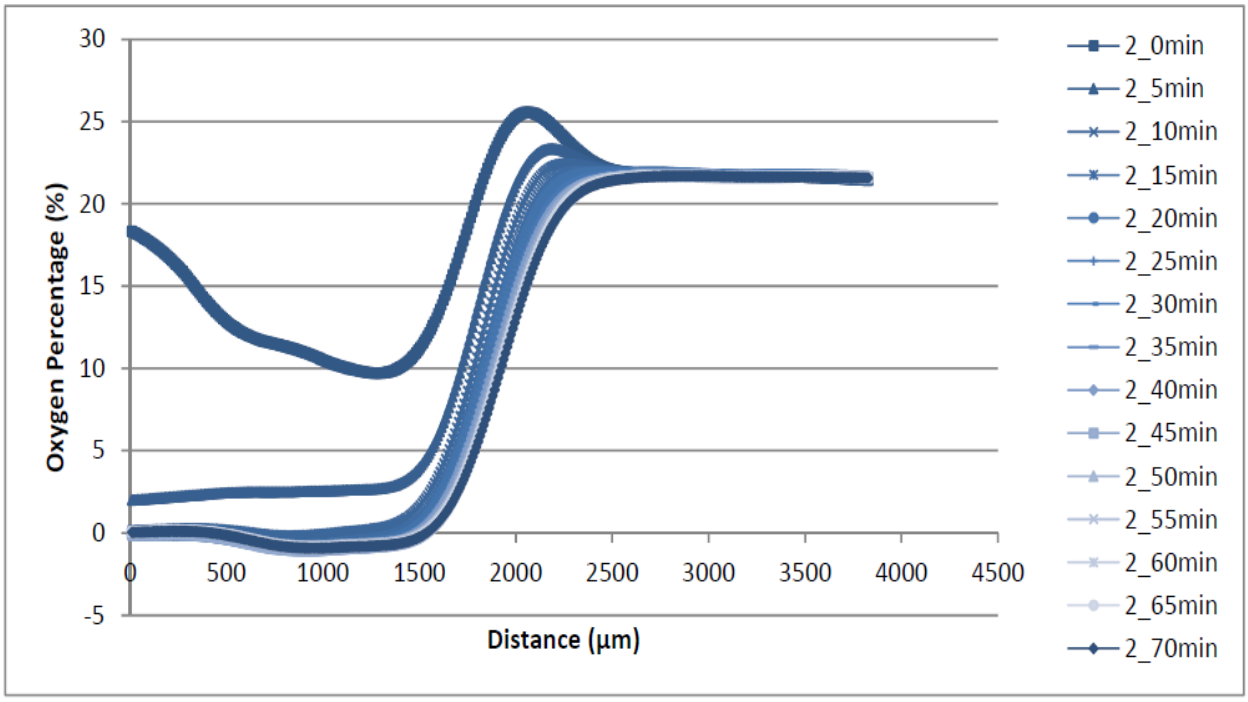
Oxygen Percentage (%)
30
25
20
15
10
5
0
-5
0
500
1000
1500
2000
2500
3000
3500
4000
4500
Distance (µm)
2_0min
2_5min
2_10min
2_15min
2_20min
2_25min
2_30min
2_35min
2_40min
2_45min
2_50min
2_55min
2_60min
2_65min
2_70min

C)

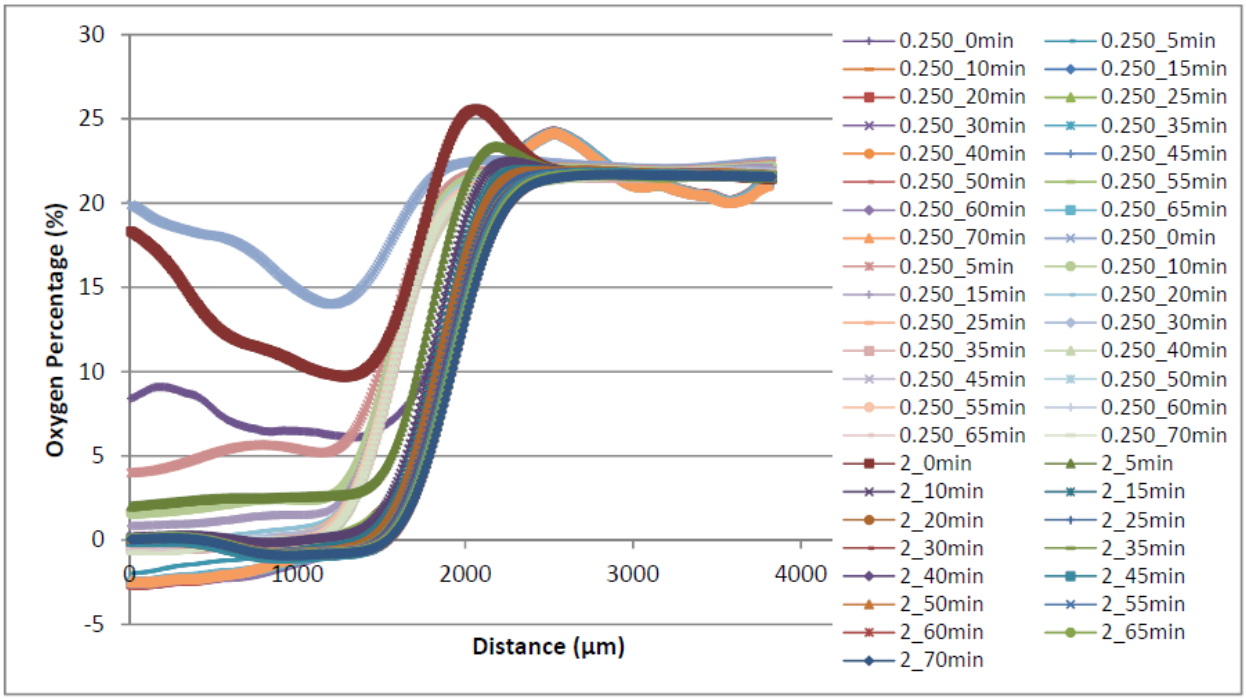

Figure 3.7. Open-well channel slow flow plots. A) Plots of 0.250mm spacing open-well channel over a 70 minute time course at 10mL/min flow. B) Plots of 2mm spacing open-well channel over a 70 minute time course at 10mL/min flow. C) Combined plot of spacing open-well channel devices over a 70 minute time course at 5 minute intervals at 10mL/min flow.

CHAPTER IV: DISCUSSION

4.1 Serpentine channel analysis

The expected results for the serpentine channel devices was that there would be a substantial difference in the oxygen gradient slope profiles depending on the parameter that was changed. It was expected that the parameters that decreased the resistance in the devices would give a lower slope value indicating that the gradient slope would be more gradual. The deeper channel devices were expected to show significant differences because the channel depth was a factor in the resistance in the devices. However, there seemed to be no significant difference shown in the smallest 10mm span devices and the largest 40mm span devices, regardless of the 140μm and 265μm depths. In the combined plot, it was observed that the oxygen gradient slope seemed to be the same. The spacing devices were also expected to give different oxygen profiles depending on the spacing distance between the normoxic and hypoxic regions of the device, since the distance the oxygen would have to diffuse across the membrane to generate a gradient varied. However, there was no significant difference observed, and again the oxygen gradient slope was observed to be the same across all spacing channels: 0.250mm, 1mm, and 2mm devices. Lastly, it was expected that changing the width of the channels would contribute to a significantly lower resistance in the channels thus showing a lower slope value for the gradient profile. However, the 0.075mm and the 0.750mm devices gave the same oxygen profile when observing the gradient slope at the dual gas condition. The devices with varying thicknesses of PDMS poured onto the master was expected to not show any significant difference, regardless of the amount of PDMS poured on the master. This was expected because the PDMS thickness of the channel layer would not change the actual channels themselves. The 1 and 2mm thickness devices gave consistent results, but the 4mm result seemed to give inconsistencies across each device. The

thickness of 4mm seemed to hit an upper threshold of focus that the microscope was capable of giving a clear image of. A combined plot for all the serpentine channel devices is shown in Figure 4.1 to show that there was a constant observed slope value for the gradients across all parameters and conditions. The same observed gradient slope across all of the parameters hinted that the resistance in the channels was not the driving force behind a change in the oxygen gradient profile. However, to confirm this lack of correlation, the open-well channel devices were also tested.

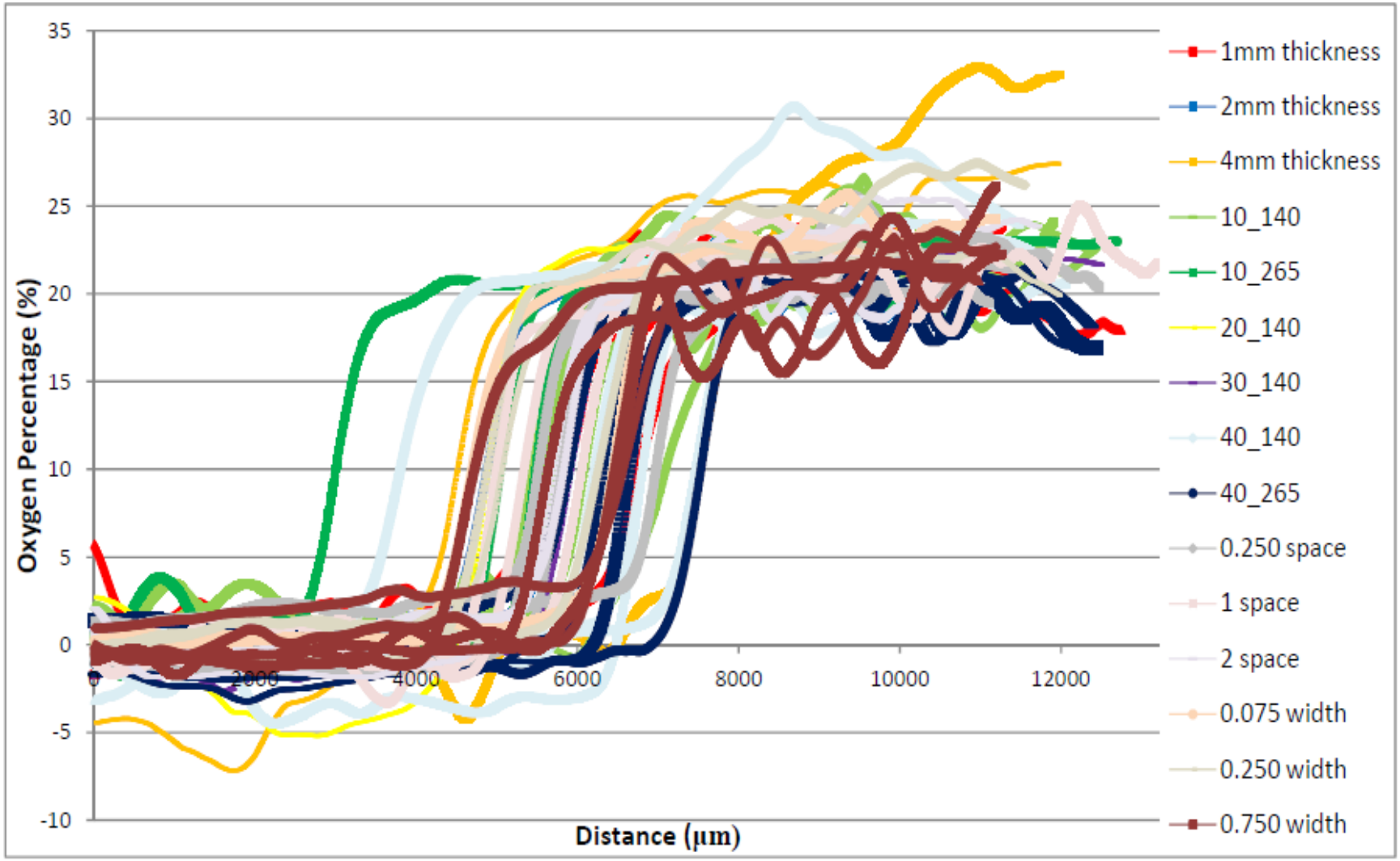

. **Figure 4.1.** Master plot showing all serpentine channel device parameters

4.2 Open-well channel analysis

In the open-well channel device design, there was expected to be a blatantly obvious difference in the gradient slope incidences from the difference in spacing between the hypoxic and normoxic regions. Because this design gave a substantially reduced resistance in the channels for the gas to flow into, the gradient manipulation was expected to be able to happen in these devices. However, the combined plot in Figure 3.5 shows that the profile is the same for the smallest spacing of 0.250mm and the largest spacing of 2mm. The time lapse experiments performed were expected to show a substantial shift in the amount of time that it took for the device to equilibrate at the dual condition. However, each device seemed to equilibrate relatively quickly around 5-10 minutes after being connected to the dual condition. A slower flow was performed to continue to try to reduce the amount of resistance in the channels showed similar results to the time lapse study. A plot of the slow flow of 10 mL/min and the fast flow of 30 mL/min (used in the serpentine channels) is shown in Figure 4.2 to indicate the fast equilibration and the identical oxygen gradient slope profiles observed in the open-well channel design.

Figure 4.2. Slow and fast flow plots for open-well channel device. A) Plots for 0.250mm gap space open-well device. B) Plots for 2mm gap space open-well device.

A)

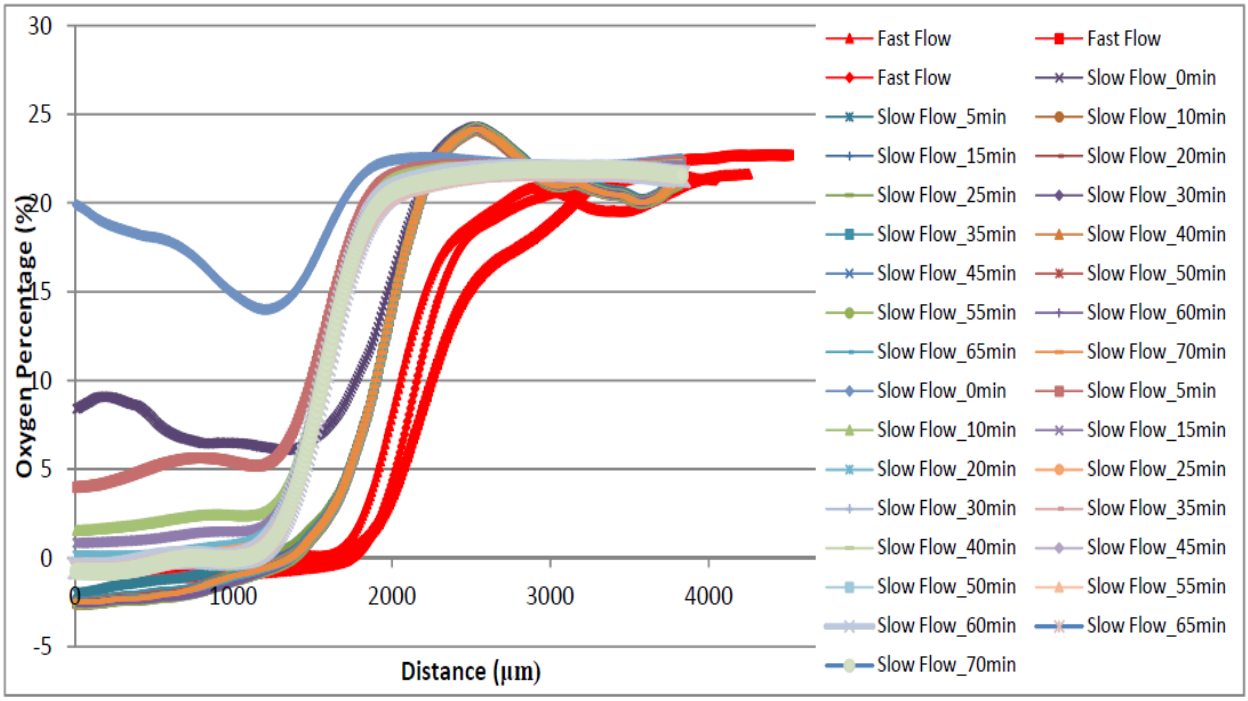
Oxygen Percentage (%)
Distance (µm)
30
25
20
15
10
5
0
-5
0
1000
2000
3000
4000
Fast Flow
Fast Flow
Fast Flow
Slow Flow_0min
Slow Flow_5min
Slow Flow_10min
Slow Flow_15min
Slow Flow_20min
Slow Flow_25min
Slow Flow_30min
Slow Flow_35min
Slow Flow_40min
Slow Flow_45min
Slow Flow_50min
Slow Flow_55min
Slow Flow_60min
Slow Flow_65min
Slow Flow_70min
Slow Flow_0min
Slow Flow_5min
Slow Flow_10min
Slow Flow_15min
Slow Flow_20min
Slow Flow_25min
Slow Flow_30min
Slow Flow_35min
Slow Flow_40min
Slow Flow_45min
Slow Flow_50min
Slow Flow_55min
Slow Flow_60min
Slow Flow_65min
Slow Flow_70min

B)

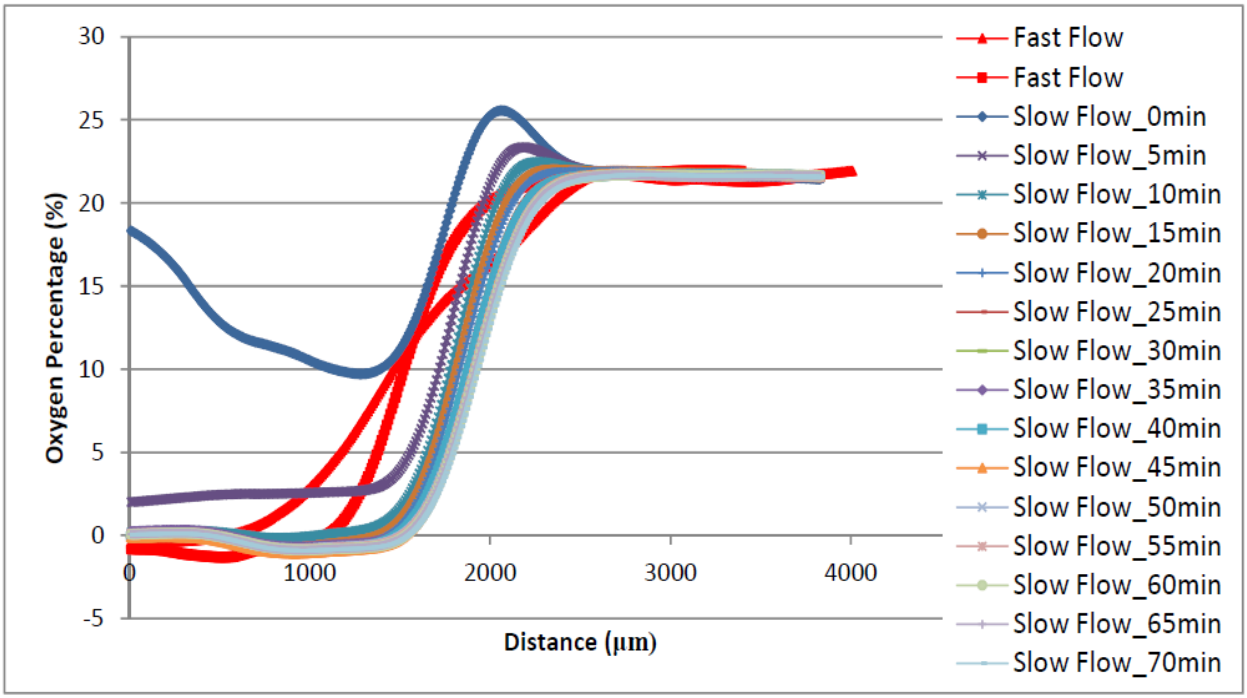
Oxygen Percentage (%)
Distance (µm)
30
25
20
15
10
5
0
-5
0
1000
2000
3000
4000
Fast Flow
Fast Flow
Slow Flow_0min
Slow Flow_5min
Slow Flow_10min
Slow Flow_15min
Slow Flow_20min
Slow Flow_25min
Slow Flow_30min
Slow Flow_35min
Slow Flow_40min
Slow Flow_45min
Slow Flow_50min
Slow Flow_55min
Slow Flow_60min
Slow Flow_65min
Slow Flow_70min

4.3 Serpentine and open-well comparison

In comparing the serpentine channel device with the open-well channel device, since only the gap spacings were observed in the open-well channel device, that parameter is compared across the two different designs. As shown in Figure 4.3 below, there seems to be very little if any difference in the oxygen gradient profiles examined in both devices. If there is a difference, it is too miniscule to be considered significant. From this conclusion, it furthers the assumption that there does not seem to be a way to manipulate the gradient by changing the design of the device at the micro-scale.

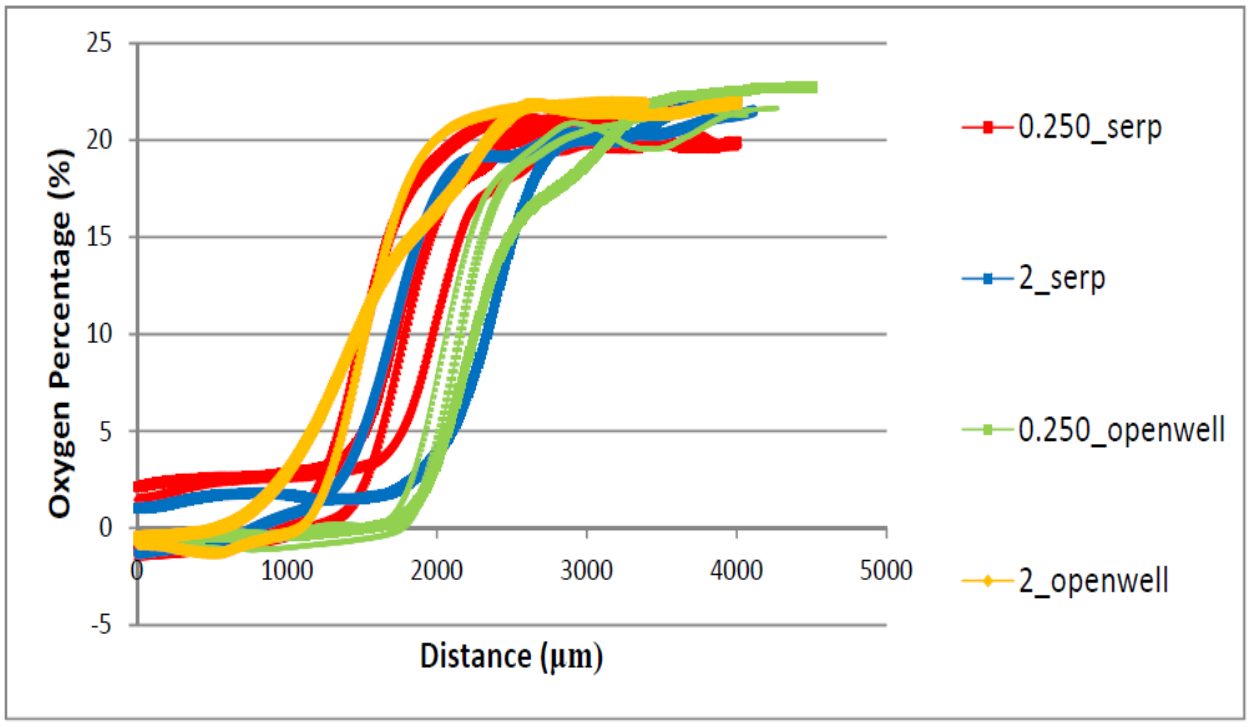

Figure 4.3. Serpentine and open-well channel gap spacing plots.

4.4 Future experiments

From the experiments performed in this study, there does not seem to be a way to precisely manipulate the oxygen gradient slope using standard oxygen tanks by changing the design parameters or the gas flowed into the device. However, future experiments could explore an extremely slow flow rate to see if that contributes to a changing oxygen gradient profile. However, it seems that a more precise way to measure this flow other than the rotometers used for this experiment must be used to precisely record the flow used in the device. Several other design iterations can be performed with a slant channel design with chamber spacings ranging from 0.250mm to up to 2cm. This design would show all the spacing experiments in the low-resistance open-well device and could examine an upper threshold of the distance where a gradient is generated. From the results of this study, it seems that the device's oxygen gradient profile cannot be manipulated at the micro-scale as a result of device design manipulation. Based on the theory that these devices' oxygen gradients cannot be changed because of the device size, future experiments can test devices scaled up to larger magnitudes to observe whether or not this will allow for oxygen profile manipulation. A study showing the threshold of the device size to be able to manipulate this oxygen profile could be performed, assuming that there are no other factors that can contribute to the oxygen profile in microfluidics.

CHAPTER V: CONCLUSION

The use of microfluidic devices and lab-on-a-chip diagnostic devices is becoming more prevalent for biologic researchers. Microfluidics offers a platform for precision control and manipulation that is an accurate representation of *in vivo* biological systems. The increasingly widespread use of PDMS as a platform for microfluidics is a result of its versatility and adaptability as well as its ability for fast prototyping. An understanding of hypoxic conditions is essential to the study of biologic systems. However, it is important to note that the body does not only function under complete hypoxia or complete normoxia. Rather, it is a mixture of different oxygen percentages and incidences of oxygen gradients in different regions of the body. The need for a universal platform that can create oxygen gradients and different gas concentrations is growing. Current solutions rely on commercially available oxygen tanks that have very specific and basic gas mixtures. The more specialized tanks are often more expensive because of the difficulty in creating the mixture. In the research field where multiple experiments are essential, the expenses accumulated for specially mixed gas tanks may become exorbitant.

The intent of this study was to examine and manipulate the oxygen gradient profile using 0% O_2 and 21% O_2 tanks to create hypoxic and normoxic environments, respectively. By examining how a change in the parameters of the microfluidic device design affected the oxygen gradient profiles, a more precise understanding and ability to manipulate the gradient profile could be achieved. However, as this study extensively showed, there seems to be no difference in the oxygen gradient profiles based on the different parameters that were examined: span, thickness, spacing, and width. Even the profiles examined in the open-well chamber designs that had a

substantially decreased resistance in the channels showed similar oxygen gradient profiles. From these experiments, it seems that this gradient is constant throughout the different devices, even with the different design factors. A possible explanation for this could be that this gradient profile is constant for devices on this scale at the micro-level. It is possible that the resistances observed in the serpentine channel devices and the open-well chamber devices do not have a significant or substantial difference to be able to create different gradient profiles. Even with an open-well chamber device and a slow flow in the channels, the device quickly equilibrates and the PDMS causes the gases to diffuse and create the same profile, regardless of the design.

Though this is not what was expected from this set of experiments, it is an interesting finding to note that there seems to be no way to create different gradient profiles by utilizing substantially different designs. Despite the intent to be able to manipulate these gradient profiles using standard gas tanks, knowing that there seems to be no way to manipulate the gradient using different designs and flow rates contributes to the understanding of the microfluidic channels and suggests that the oxygen manipulation must be achieved in a different manner.

CITED LITERATURE

1. Nguyen, N. T., & Wereley, S. T. (2002). *Fundamentals and applications of microfluidics*. Artech House.

2. Whitesides, G. M. (2006). The origins and the future of microfluidics. *Nature,442*(7101), 368-373.

3. Stone, H. A., Stroock, A. D., & Ajdari, A. (2004). Engineering flows in small devices: microfluidics toward a lab-on-a-chip. *Annu. Rev. Fluid Mech., 36*, 381-411.

4. Blake, A. J., Pearce, T. M., Rao, N. S., Johnson, S. M., & Williams, J. C. (2007). Multilayer PDMS microfluidic chamber for controlling brain slice microenvironment. *Lab on a Chip*, *7*(7), 842-849.

5. Massey, L. K. Permeability and Other Film Properties of Plastics and Elastomers: A Guide to Packaging and Barrier Materials, 2nd ed.; William Andrew Inc.: Norwich, NY, 2003

6. Oppegard, S. C., Nam, K. H., Carr, J. R., Skaalure, S. C., & Eddington, D. T. (2009). Modulating temporal and spatial oxygenation over adherent cellular cultures. *PloS one*, *4*(9), e6891.

7. Lötters, J. C., Olthuis, W., Veltink, P. H., & Bergveld, P. (1997). The mechanical properties of the rubber elastic polymer polydimethylsiloxane for sensor applications. *Journal of Micromechanics and Microengineering*, *7*(3), 145.

8. Heo YS, Cabrera LM, Song JW, Futai N, Tung YC, et al. (2007) Characterization and resolution of evaporation-mediated osmolality shifts that constrain microfluidic cell culture in poly(dimethylsiloxane) devices. Analytical Chemistry 79: 1126–1134.

9. Randall GC, Doyle PS (2005) Permeation-driven flow in poly(dimethylsiloxane) microfluidic devices. Proceedings of the National Academy of Sciences of the United States of America 102: 10813–10818.

10. Roman GT, Hlaus T, Bass KJ, Seelhammer TG, Culbertson CT (2005) Sol-gel modified poly(dimethylsiloxane) microfluidic devices with high electroosmotic mobilities and hydrophilic channel wall characteristics. Analytical Chemistry 77: 1414–1422.

11. Mukhopadyay R (2007) When PDMS isn't the best. Analytical Chemistry 79: 3248–3253.

12. Clarson, S. J., & Semlyen, J. A. (1993). *Siloxane polymers*. Prentice Hall.

13. ABCR 1994 Research Chemicals and Metals Catalogue Karlsruhe, Germany.

14. van Krevelen D W and Hoftyzer P J 1976 Properties of Polymers (Amsterdam: Elsevier)

15. McDonald JC, Duffy DC, Anderson JR, Chiu DT, Wu H, Schueller OJ, Whitesides GM. Fabrication of microfluidic systems in poly(dimethylsiloxane) Electrophoresis. 2000;21:27-40.

16. Whitesides, G.M., Ostuni, E., Takayama, S., Jiang, X. and Ingber, D.E., Soft lithography in biology and biochemistry. Annu. Rev. Biomed. Eng., 2001. 3: p. 335-373.

17. Harris, A. L. (2002). Hypoxia—a key regulatory factor in tumour growth.*Nature Reviews Cancer*, *2*(1), 38-47.

18. Mohyeldin, A., Garzón-Muvdi, T., & Quiñones-Hinojosa, A. (2010). Oxygen in stem cell biology: a critical component of the stem cell niche. *Cell stem cell*, *7*(2), 150-161.

19. Brennan, M. D., Rexius-Hall, M. L., Elgass, L. J., & Eddington, D. T. (2014). Oxygen control with microfluidics. *Lab on a Chip*, *14*(22), 4305-4318.

20. Ke, Q., & Costa, M. (2006). Hypoxia-inducible factor-1 (HIF-1). *Molecular pharmacology*, *70*(5), 1469-1480.

21. Semenza, G. L. (2001). Hypoxia-inducible factor 1: oxygen homeostasis and disease pathophysiology. *Trends in molecular medicine*, *7*(8), 345-350.

22. Simon, M. C., & Keith, B. (2008). The role of oxygen availability in embryonic development and stem cell function. *Nature reviews Molecular cell biology*, *9*(4), 285-296.

23. Fraisl, P., Mazzone, M., Schmidt, T., & Carmeliet, P. (2009). Regulation of angiogenesis by oxygen and metabolism. *Developmental cell*, *16*(2), 167-179.

24. Balin, A. K., Fisher, A. J., & Carter, D. M. (1984). Oxygen modulates growth of human cells at physiologic partial pressures. *The Journal of experimental medicine*, *160*(1), 152-166.

25. Decaris, M. L., Lee, C. I., Yoder, M. C., Tarantal, A. F., & Leach, J. K. (2009). Influence of the oxygen microenvironment on the proangiogenic potential of human endothelial colony forming cells. *Angiogenesis*, *12*(4), 303-311.

26. Allen, J. W., & Bhatia, S. N. (2003). Formation of steady-state oxygen gradients in vitro: Application to liver zonation. *Biotechnology and bioengineering*, *82*(3), 253-262.

27. Huh, D., Fujioka, H., Tung, Y. C., Futai, N., Paine, R., Grotberg, J. B., & Takayama, S. (2007). Acoustically detectable cellular-level lung injury induced by fluid mechanical stresses in microfluidic airway systems.*Proceedings of the National Academy of Sciences*, *104*(48), 18886-18891.

28. Kamotani, Y., Bersano-Begey, T., Kato, N., Tung, Y. C., Huh, D., Song, J. W., & Takayama, S. (2008). Individually programmable cell stretching microwell arrays actuated by a Braille display. *Biomaterials*, *29*(17), 2646-2655.

29. Song, J. W., Cavnar, S. P., Walker, A. C., Luker, K. E., Gupta, M., Tung, Y. C., ... & Takayama, S. (2009). Microfluidic endothelium for studying the intravascular adhesion of metastatic breast cancer cells. *PloS one*, *4*(6), e5756.

30. Kim, S., Kim, H. J., & Jeon, N. L. (2010). Biological applications of microfluidic gradient devices. *Integrative Biology*, *2*(11-12), 584-603.

31. Douville, N. J., Zamankhan, P., Tung, Y. C., Li, R., Vaughan, B. L., Tai, C. F., ... & Takayama, S. (2011). Combination of fluid and solid mechanical stresses contribute to cell death and detachment in a microfluidic alveolar model. *Lab on a chip*, *11*(4), 609-619.

32. Rexius-Hall, M. L., Mauleon, G., Malik, A. B., Rehman, J., & Eddington, D. T. (2014). Microfluidic platform generates oxygen landscapes for localized hypoxic activation. *Lab on a chip*, *14*(24), 4688-4695.

33. Mehta, G., Lee, J., Cha, W., Tung, Y. C., Linderman, J. J., & Takayama, S. (2009). Hard top soft bottom microfluidic devices for cell culture and chemical analysis. *Analytical chemistry*, *81*(10), 3714-3722.

34. Sia, Samuel K., and Larry J. Kricka. "Microfluidics and point-of-care testing."*Lab on a Chip* 8, no. 12 (2008): 1982-1983.

35. Allen, C. B., Schneider, B. K., & White, C. W. (2001). Limitations to oxygen diffusion and equilibration in in vitro cell exposure systems in hyperoxia and hypoxia. *American Journal of Physiology-Lung Cellular and Molecular Physiology*, *281*(4), L1021-L1027.

36. Mehta, G., Mehta, K., Sud, D., Song, J. W., Bersano-Begey, T., Futai, N., ... & Takayama, S. (2007). Quantitative measurement and control of oxygen levels in microfluidic poly (dimethylsiloxane) bioreactors during cell culture.*Biomedical microdevices*, *9*(2), 123-134.

37. Adler, M., Polinkovsky, M., Gutierrez, E., & Groisman, A. (2010). Generation of oxygen gradients with arbitrary shapes in a microfluidic device. *Lab on a Chip*, *10*(3), 388-391.

38. Chen, Y. A., King, A. D., Shih, H. C., Peng, C. C., Wu, C. Y., Liao, W. H., & Tung, Y. C. (2011). Generation of oxygen gradients in microfluidic devices for cell culture using spatially confined chemical reactions. *Lab on a Chip*,*11*(21), 3626-3633.

39. Sinkala, E., & Eddington, D. T. (2010). Oxygen sensitive microwells. *Lab on a Chip*, *10*(23), 3291-3295.

40. Anderson, J.R., Chiu, D.T., Jackman, R.J., Cherniavskaya, O., McDonald, J.C., Wu, H., Whitesides, S.H. and Whitesides, G.M., Fabrication of topologically complex threedimensional microfluidic systems in PDMS by rapid prototyping. Anal. Chem., 2000. 72: p. 3158-3164.

41. Zhong, W., Urayama, P., & Mycek, M. A. (2003). Imaging fluorescence lifetime modulation of a ruthenium-based dye in living cells: the potential for oxygen sensing. *Journal of Physics D: Applied Physics*, *36*(14), 1689.

APPENDIX A: Triangle smoothing MATLAB function

When analyzing the oxygen percentage data that was the output from the Stern-Volmer function run in MATLAB, there appeared to be varying degrees of noise generated from the fluorescence imaging of the PtOEPK sensor. Since it was important for this project to have a clear viewpoint of the gradient and the oxygen plateaus, the data was filtered to get rid of the noise. The data was run through a bandpass filter using a triangular pulse function with a window of L=81. However, other window sizes were observed to examine the best threshold for the cutoff used in the filter.

Below is an example of a raw data set that was the output of the Stern-Volmer function and the process of generating the smoothed function using the triangle-filter.

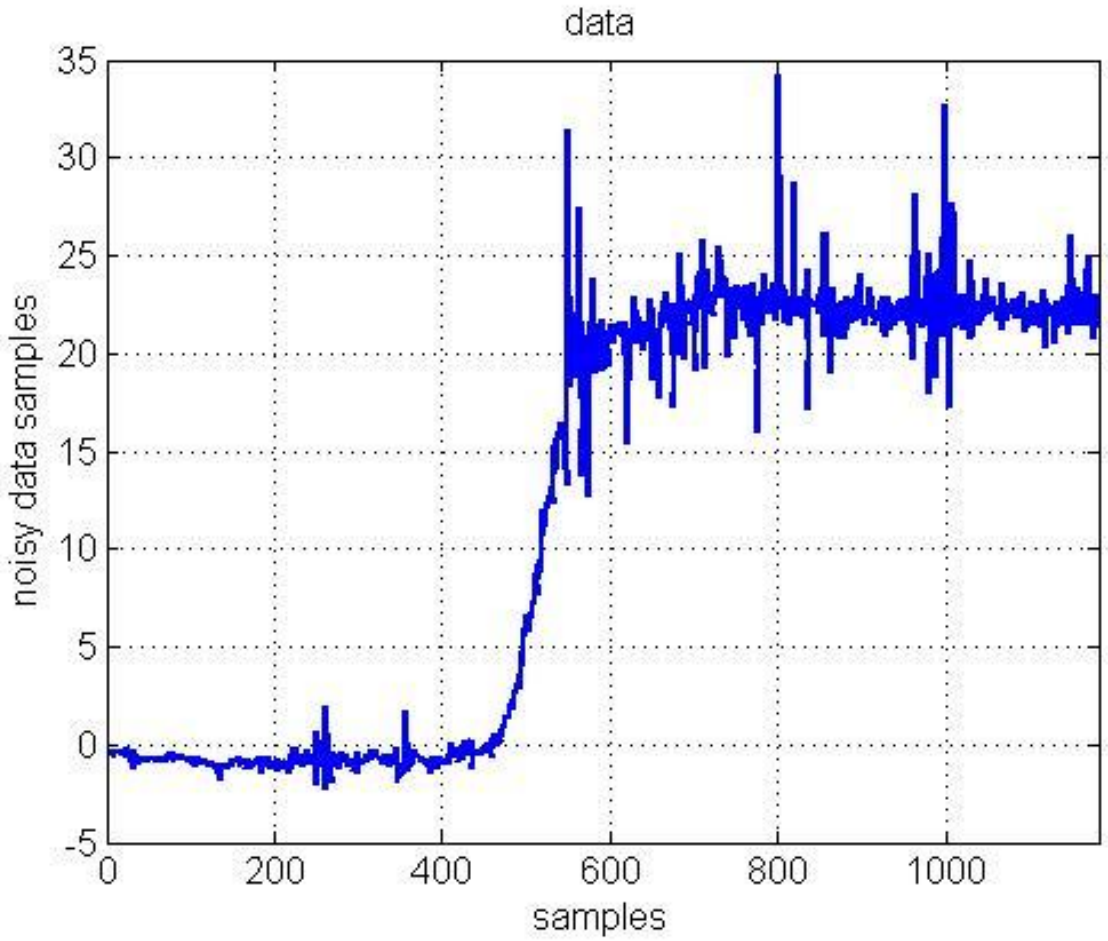

APPENDIX A (continued)

The next figure shows the different window sizes being examined to choose the best one for the triangle smoothing.

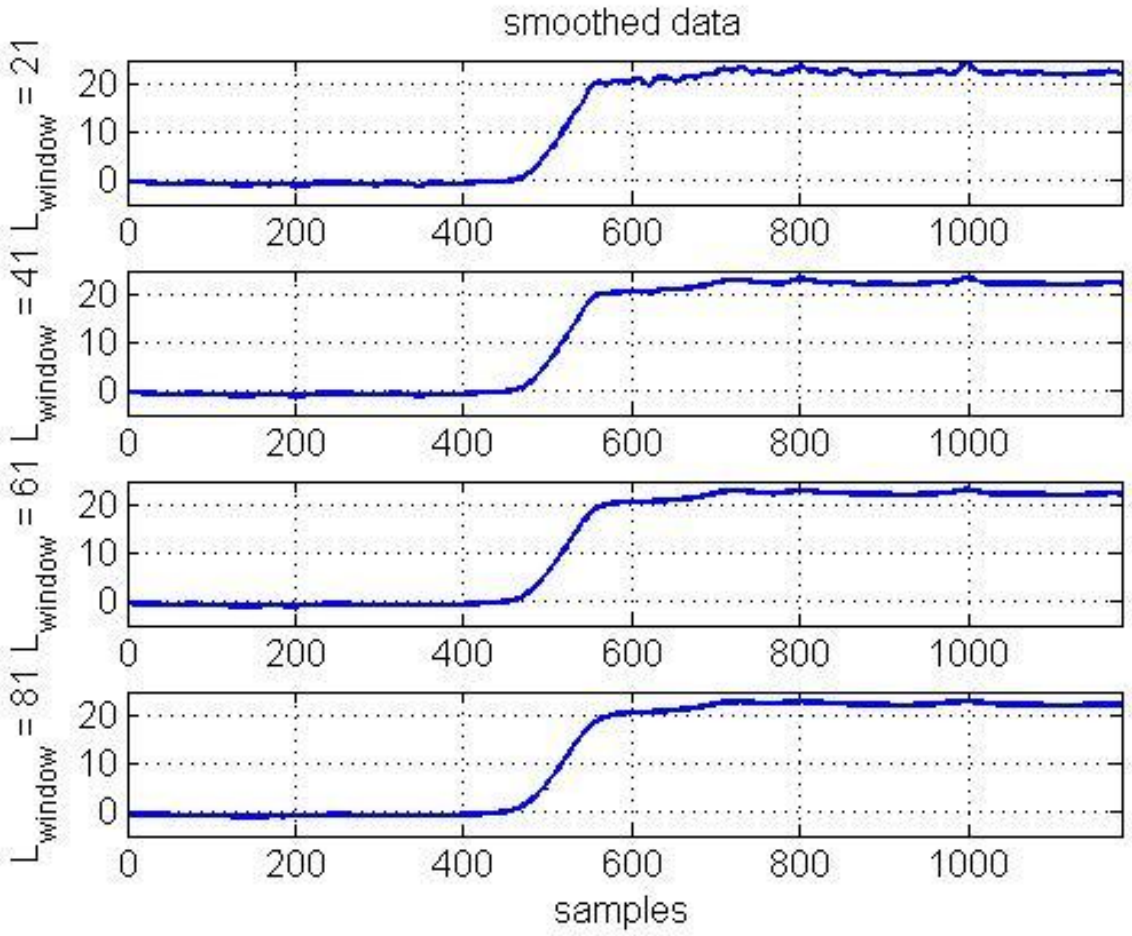

APPENDIX A (continued)

The last figure shows the chosen window L = 81 and the histogram to show the generated plateaus for this particular curve as an attempt to standardize the slope calculation. This information was important when the slopes were calculated manually, but this was later disregarded because there was too much variability and human error.

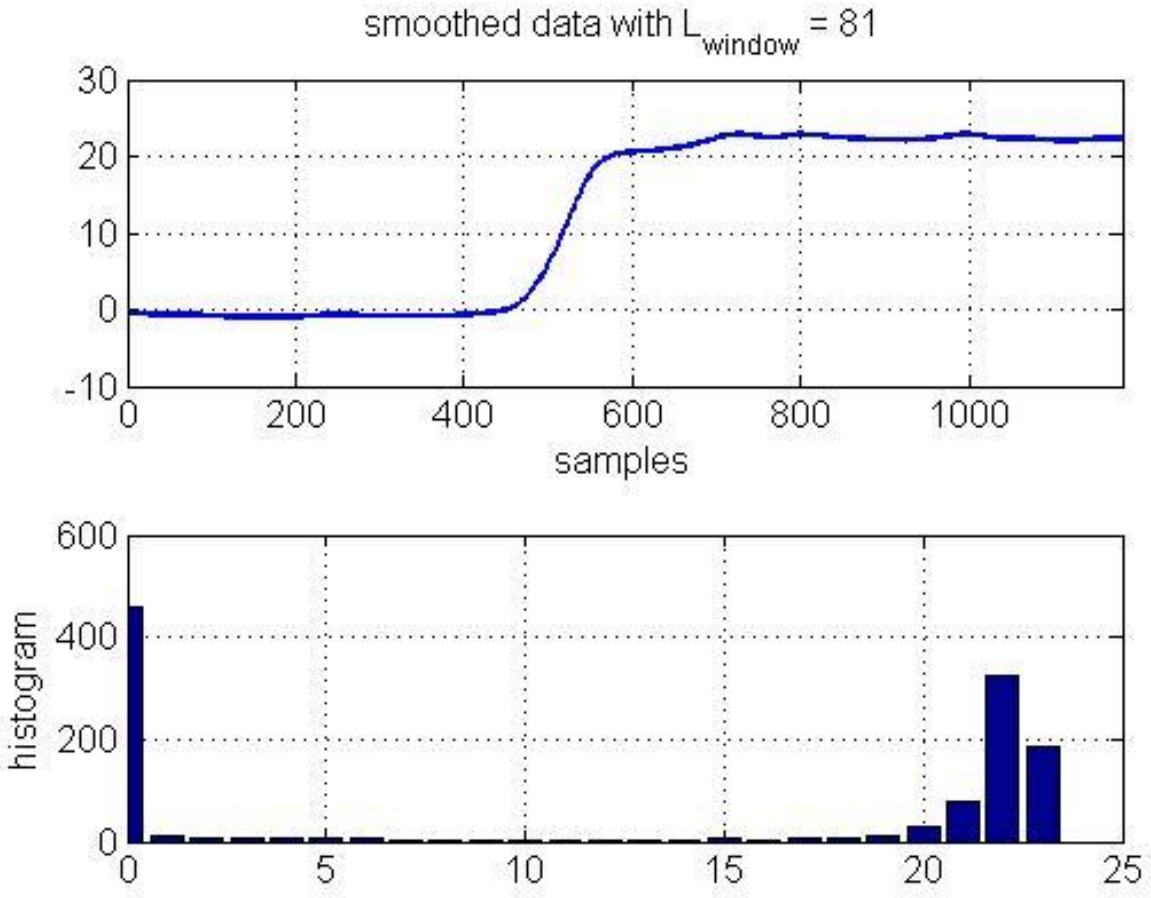

The code is provided here for reference. The first part is the function to create a triangle window based on the given signal and the specified window size. This function is used in the second code provided to actually generate the smoothed curve and histogram to generate the figures shown above. The portion that is commented out in the smoothing function was used to find the slope value based on the histogram function, but was taken out in favor of visual analysis instead.

APPENDEX A (continued)

Triangle window function MATLAB code:

```
function sm_signal = function_triangle_window(signal, Wlng)
signal = signal(:); %makes signal into a column vector

if rem(Wlng, 2)==0, Wlng = Wlng + 1; end %making window an odd number
Wlng2f = floor(Wlng/2);
trild = triang(Wlng);

row = size(signal, 1); %setting size to the same as column vector size

templ = zeros(row, 1); %creates a vector of zeros
inx_column = find(signal~=0);
if ~isempty(inx_column), templ(inx_column(1):inx_column(end)) = 1; end

temp = zeros(row+2*Wlng2f, 1);
temp(Wlng2f+1:Wlng2f+row,1) = templ;

data = zeros(size(temp));
data(Wlng2f+1:Wlng2f+row,1) = signal; %inserts 0s in the front and back of data

sm_signal = zeros(size(data)); %resolving memory
inx_column = find(data~=0); %finds indexes where data is not 0
for kl=inx_column(1):inx_column(end), %looping through data to find weighted sum
    windowed_data = data(kl-Wlng2f:kl+Wlng2f,1);
    windowed_temp = temp(kl-Wlng2f:kl+Wlng2f,1);
    weighted_data = windowed_data .* trild;
    weights = windowed_temp .* trild;
    sm_signal(kl,1) = sum(weighted_data) / sum(weights);
end

sm_signal = sm_signal(Wlng2f+1:Wlng2f+row); %smoothed data points
return
```

APPENDIX A (continued)

Smoothing function MATLAB code (part 1):

```
clear; clc; close all

font_size = 12; font_axes = 12;

%% load a data file
data = xlsread('E:\BML Data\Updated 021016\BML\Raw Data\Serpentine Channels\092515\0.250↙
Width\ES092515Wstar_01_oxygenpercent.xlsx');

signal = data(:,1); %setting data as a column matrix
N = length(signal); %size of data
sample_index = (1:N); %indexing through values for x-axis
idx = find(isnan(signal)==1); %finds values that are "NAN"
if ~isempty(idx),
    signal(idx) = []; sample_index(idx) = []; %sets NAN cells to empty and index values↙
to an empty cell
    signal = interp1(sample_index, signal, (1:N), 'linear'); %fills in empty cells to↙
linear interpolation values
end

figure(1), clf; plot(signal, 'linewidth', 2); grid; %figure 1 plots original signal with↙
outliers replaced by interpolation values
    title('data', 'fontsize', font_size); ylabel('noisy data samples', 'fontsize',↙
font_size);
    xlabel('samples', 'fontsize', font_size); set(gca, 'fontsize', font_axes);
    set(gca, 'xlim', [0, N]); drawnow %sets x-axis to size of signal

%% apply a triangular window to smooth the data: low-pass filter to suppress noise
figure(2), clf;
for kk=1:4,
    if kk==1,
        Wlng = 21; % length of the triangular window to examine best triangle window↙
value
    elseif kk==2,
        Wlng = 41;
    elseif kk==3,
        Wlng = 61;
    elseif kk==4,
        Wlng = 81;
    end

    sm_signal = function_triangle_window(signal, Wlng); %plot for different triangle↙
window values to compare
    figure(2), subplot(4,1,kk), plot(sm_signal, 'linewidth', 2); grid;
        if kk==1,
            title('smoothed data', 'fontsize', font_size);
        elseif kk==4,
            xlabel('samples', 'fontsize', font_size);
        end
        ylabel(['L_{window} = ', num2str(Wlng)], 'fontsize', font_size);
     set(gca, 'fontsize', font_axes); set(gca, 'xlim', [0, N]);
     set(gca, 'ylim', [-5 25]); drawnow
```

APPENDIX A (continued)

Smoothing function MATLAB code (part 2):

```
end

%% decide the window length based on Figure 2 and estimate the slope
Wlng = 81; %setting windo length
sm_signal = function_triangle_window(signal, Wlng); %setting signal to the smoothed
signal
hist_bins = (0:1:25); Nhist_bins = length(hist_bins); %creates range for histogram
Nhist = hist(sm_signal, hist_bins); %plots histogram based on previous values
figure(3), subplot(211), plot(sm_signal, 'linewidth', 2); grid; %plots filtered signal
        title(['smoothed data with L_{window} = ', num2str(Wlng)], 'fontsize',
font_size);
        xlabel('samples', 'fontsize', font_size);
        set(gca, 'fontsize', font_axes); set(gca, 'xlim', [0, N]); drawnow
    subplot(212), bar(hist_bins, Nhist); grid; %plots histogram (bar function controls
the histogram plot)
        ylabel('histogram', 'fontsize', font_size);
        set(gca, 'fontsize', font_axes); set(gca, 'xlim', [0, max(hist_bins)]); drawnow

Nhist_bins2 = floor(Nhist_bins/2); %finds center point and rounds to integer value
low_idx = find(Nhist(1:Nhist_bins2)==max(Nhist(1:Nhist_bins2))); %finding value that has
the most (lower plateau)
low_idx = low_idx(end); %if same value, picks the greater index value one
low_plateau = hist_bins(low_idx); %sets low plateau to the value found

high_idx = find(Nhist(Nhist_bins2+1:end)==max(Nhist(Nhist_bins2+1:end))); %finds value
that has the most (upper plateau)
high_idx = high_idx(1) + Nhist_bins2; %finds the actual index value (since only looking
at upper half)
high_plateau = hist_bins(high_idx); %sets upper plateau to value found

% %%
% tolerance = 0.1; %setting the value to control for window of error
% low_value = (1 + tolerance) * low_plateau;
% high_value = (1 - tolerance)* high_plateau;
% starting_point = find(sm_signal<=low_value); starting_point = starting_point(end); %
sets the starting point of the slope to the actual low value
% ending_point = find(sm_signal>=high_value); ending_point = ending_point(1); %sets the
ending point to the actual high value
% slope = (high_value - low_value) / (ending_point - starting_point); %finds the slope
%
% line_eq = slope * (starting_point:ending_point) - slope*starting_point + low_value; %
slope-intercept form
% figure(4), clf; plot((1:N), signal, 'b', ... %sets signal to blue line on the plot
%     (starting_point:ending_point), line_eq, 'r--', (1:N), sm_signal, 'g', 'linewidth',
2); grid; %red line is the slope found. green is smoothed data
%     title(['data: slope = ', num2str(slope)], 'fontsize', font_size);
%     ylabel('noisy data samples', 'fontsize', font_size);
%     xlabel('samples', 'fontsize', font_size); set(gca, 'fontsize', font_axes);
%     set(gca, 'xlim', [0, N]); set(gca, 'ylim', [-5 35]); drawnow
%
%     %%
```

APPENDIX A (continued)

Smoothing function MATLAB code (part 3):

```
% figure(5), clf; plot((1:N), sm_signal, 'b', ... %sets smoothed signal to blue line on↙
the plot
%     (starting_point:ending_point), line_eq, 'r--', 'linewidth', 2); grid; %red line is↙
the slope found
%     title(['data: slope = ', num2str(slope)], 'fontsize', font_size);
%     ylabel('noisy data samples', 'fontsize', font_size);
%     xlabel('samples', 'fontsize', font_size); set(gca, 'fontsize', font_axes);
%     set(gca, 'xlim', [0, N]); set(gca, 'ylim', [-5 35]); drawnow


return
```

VITA

Esther Jeeyoung Shin

EDUCATION

8/14-5/16 **University of Illinois at Chicago College of Engineering**
Chicago, IL
M.S. Bioengineering, Thesis Option

8/09-5/14 **Georgia Institute of Technology**
Atlanta, GA
B.S. Biomedical Engineering, Research Option

RESEARCH EXPERIENCE

8/14-5/16 **Graduate Researcher**
University of Illinois at Chicago Bioengineering
Chicago, IL

Conducting research to explore the manipulation of oxygen gradients in microfluidic PDMS devices using normoxic and hypoxic conditions. By gaining an understanding of the factors that affect the slope of the oxygen gradients in the devices, future devices can be designed to precisely manipulate oxygen gradient profiles to accurately explore its role in biological processes such as stem cell differentiation, angiogenesis, and many others.

09/13-05/14 **Undergraduate Researcher**
Georgia Institute of Technology School of Biology
Atlanta, GA

Conducted research exploring the uptake of exosomes into ovarian cancer hey cells using constructed microfluidic PDMS devices. Explored using microfluidic devices for live cell imaging techniques to observe the real-time uptake of exosomes into the cells. Research expanded on the potential to utilize exosomes in gene therapy and imitate real cellular environments.

01/10-05/13 **Undergraduate Researcher**
Georgia Institute of Technology School of Applied Physiology
Atlanta, GA

Assisted in the data digitization of rat limb kinematics data to quantify the joint angles and movement. 8 different points were specified on the x-ray images of a rat's movements (hip, knee, ankle, etc.) and designated over 1,500 frames in over 120 rats. Data analysis was performed to assist in research on nerve and signal analysis in the rat's physiological compensatory movements. Conducted an independent project that worked on overlaying x-ray images and MRI images to compose a 3-dimensional working model of the rat's movements (commonly referred to as x-ray of moving morphology or XROMM).

12/10-05/11 **Undergraduate Research Assistant**
Georgia Institute of Technology SciTrain University
Atlanta, GA

SciTrain University focused on the accessibility and improvement of teaching in science and technology (STEM) courses. Provided feedback to the instructors of specific courses to improve teaching methods and directed focus groups of students to narrow the gap between instructors and students. Data was transcribed and coded to quantify the verbal observation data.

TEACHING EXPERIENCE

08/15-12/15 **Teaching Assistant, BioE 101 Introductory Course**
University of Illinois at Chicago, Department of Bioengineering
Chicago, IL

Provided assistance for approximately 90 students in the bioengineering undergraduate introduction course. Answered questions and offered help in Arduino coding and wiring, Solidworks, technical writing, and miscellaneous tasks.

02/15-present **4th Grade Sunday School Teacher**
Hebron Presbyterian Church
Mount Prospect, IL

In charge of planning lessons consisting of the Bible lesson learned on that day as well as an activity or game to apply for a class of 8 fourth grade students. Supervise around 60 elementary students each week during Sunday service and following service before they are picked up by their parents.

08/13-12/13 **Teaching Assistant, Clinical Observation and Design Experience (CODE)**
Georgia Institute of Technology, Department of Biomedical Engineering
Atlanta, GA

Provided feedback and grading from an engineering perspective for students taking the clinical observation course. The course placed engineering students in the emergency department at two separate hospitals and challenged students to observe and suggest changes from an engineering design perspective.

08/11-05/13 **Teaching Assistant/Team Leader, GT 1000**
Georgia Institute of Technology
Atlanta, GA

Advised students with everyday problems in adjusting to college and facilitated the transitional period for freshman Georgia Tech students. Activities, games, and assignments were planned for students to gain exposure and make connect ions.

06/05-present **Self-Employed Summer Tutor**
Diamond Bar, CA

Private tutored students in the local community in math, English, and science courses during the summer.

PUBLICATIONS

Undergraduate Thesis
Shin, Esther J., *Exosome Uptake into Hey Ovarian Cancer Cells and its Potential to Serve as a Vessel for Gene Therapy.*
Advisor: Dr. Fredrik Vannberg, Georgia Institute of Technology
School of Biology, 2014.